arXiv:1208.4468v1 [hep-ex] 22 Aug 2012

DESY–12–144
August 2012

Production of the excited charm mesons D_1 and D_2^* at HERA

ZEUS Collaboration

Abstract

The production of the excited charm mesons $D_1(2420)$ and $D_2^*(2460)$ in ep collisions has been measured with the ZEUS detector at HERA using an integrated luminosity of $373\,\mathrm{pb}^{-1}$. The masses of the neutral and charged states, the widths of the neutral states, and the helicity parameter of $D_1(2420)^0$ were determined and compared with other measurements and with theoretical expectations. The measured helicity parameter of the D_1^0 allows for some mixing of S- and D-waves in its decay to $D^{*\pm}\pi^{\mp}$. The result is also consistent with a pure D-wave decay. Ratios of branching fractions of the two decay modes of the $D_2^*(2460)^0$ and $D_2^*(2460)^{\pm}$ states were measured and compared with previous measurements. The fractions of charm quarks hadronising into D_1 and D_2^* were measured and are consistent with those obtained in e^+e^- annihilations.

The ZEUS Collaboration

H. Abramowicz[45,ah], I. Abt[35], L. Adamczyk[13], M. Adamus[54], R. Aggarwal[7,c], S. Antonelli[4], P. Antonioli[3], A. Antonov[33], M. Arneodo[50], O. Arslan[5], V. Aushev[26,27,z], Y. Aushev,[27,z,aa], O. Bachynska[15], A. Bamberger[19], A.N. Barakbaev[25], G. Barbagli[17], G. Bari[3], F. Barreiro[30], N. Bartosik[15], D. Bartsch[5], M. Basile[4], O. Behnke[15], J. Behr[15], U. Behrens[15], L. Bellagamba[3], A. Bertolin[39], S. Bhadra[57], M. Bindi[4], C. Blohm[15], V. Bokhonov[26,z], T. Bołd[13], K. Bondarenko[27], E.G. Boos[25], K. Borras[15], D. Boscherini[3], D. Bot[15], I. Brock[5], E. Brownson[56], R. Brugnera[40], N. Brümmer[37], A. Bruni[3], G. Bruni[3], B. Brzozowska[53], P.J. Bussey[20], B. Bylsma[37], A. Caldwell[35], M. Capua[8], R. Carlin[40], C.D. Catterall[57], S. Chekanov[1], J. Chwastowski[12,e], J. Ciborowski[53,al], R. Ciesielski[15,h], L. Cifarelli[4], F. Cindolo[3], A. Contin[4], A.M. Cooper-Sarkar[38], N. Coppola[15,i], M. Corradi[3], F. Corriveau[31], M. Costa[49], G. D'Agostini[43], F. Dal Corso[39], J. del Peso[30], R.K. Dementiev[34], S. De Pasquale[4,a], M. Derrick[1], R.C.E. Devenish[38], D. Dobur[19,t], B.A. Dolgoshein [33,†], G. Dolinska[27], A.T. Doyle[20], V. Drugakov[16], L.S. Durkin[37], S. Dusini[39], Y. Eisenberg[55], P.F. Ermolov [34,†], A. Eskreys [12,†], S. Fang[15,j], S. Fazio[8], J. Ferrando[20], M.I. Ferrero[49], J. Figiel[12], B. Foster[38,ad], G. Gach[13], A. Galas[12], E. Gallo[17], A. Garfagnini[40], A. Geiser[15], I. Gialas[21,w], A. Gizhko[27,ab], L.K. Gladilin[34,ac], D. Gladkov[33], C. Glasman[30], O. Gogota[27], Yu.A. Golubkov[34], P. Göttlicher[15,k], I. Grabowska-Bołd[13], J. Grebenyuk[15], I. Gregor[15], G. Grigorescu[36], G. Grzelak[53], O. Gueta[45], M. Guzik[13], C. Gwenlan[38,ae], T. Haas[15], W. Hain[15], R. Hamatsu[48], J.C. Hart[44], H. Hartmann[5], G. Hartner[57], E. Hilger[5], D. Hochman[55], R. Hori[47], A. Hüttmann[15], Z.A. Ibrahim[10], Y. Iga[42], R. Ingbir[45], M. Ishitsuka[46], H.-P. Jakob[5], F. Januschek[15], T.W. Jones[52], M. Jüngst[5], I. Kadenko[27], B. Kahle[15], S. Kananov[45], T. Kanno[46], U. Karshon[55], F. Karstens[19,u], I.I. Katkov[15,l], M. Kaur[7], P. Kaur[7,c], A. Keramidas[36], L.A. Khein[34], J.Y. Kim[9], D. Kisielewska[13], S. Kitamura[48,aj], R. Klanner[22], U. Klein[15,m], E. Koffeman[36], N. Kondrashova[27,ab], O. Kononenko[27], P. Kooijman[36], Ie. Korol[27], I.A. Korzhavina[34,ac], A. Kotański[14,f], U. Kötz[15], H. Kowalski[15], O. Kuprash[15], M. Kuze[46], A. Lee[37], B.B. Levchenko[34], A. Levy[45], V. Libov[15], S. Limentani[40], T.Y. Ling[37], M. Lisovyi[15], E. Lobodzinska[15], W. Lohmann[16], B. Löhr[15], E. Lohrmann[22], K.R. Long[23], A. Longhin[39,af], D. Lontkovskyi[15], O.Yu. Lukina[34], J. Maeda[46,ai], S. Magill[1], I. Makarenko[15], J. Malka[15], R. Mankel[15], A. Margotti[3], G. Marini[43], J.F. Martin[51], A. Mastroberardino[8], M.C.K. Mattingly[2], I.-A. Melzer-Pellmann[15], S. Mergelmeyer[5], S. Miglioranzi[15,n], F. Mohamad Idris[10], V. Monaco[49], A. Montanari[15], J.D. Morris[6,b], K. Mujkic[15,o], B. Musgrave[1], K. Nagano[24], T. Namsoo[15,p], R. Nania[3], A. Nigro[43], Y. Ning[11], T. Nobe[46], D. Notz[15], R.J. Nowak[53], A.E. Nuncio-Quiroz[5], B.Y. Oh[41], N. Okazaki[47], K. Olkiewicz[12], Yu. Onishchuk[27], K. Papageorgiu[21], A. Parenti[15], E. Paul[5], J.M. Pawlak[53], B. Pawlik[12], P. G. Pelfer[18], A. Pellegrino[36], W. Perlański[53,am], H. Perrey[15], K. Piotrzkowski[29], P. Pluciński[54,an], N.S. Pokrovskiy[25], A. Polini[3], A.S. Proskuryakov[34], M. Przybycień[13], A. Raval[15], D.D. Reeder[56], B. Reisert[35], Z. Ren[11], J. Repond[1], Y.D. Ri[48,ak], A. Robertson[38], P. Roloff[15,n], I. Rubinsky[15], M. Ruspa[50], R. Sacchi[49], U. Samson[5], G. Sartorelli[4], A.A. Savin[56], D.H. Saxon[20], M. Schioppa[8], S. Schlenstedt[16], P. Schleper[22], W.B. Schmidke[35], U. Schneekloth[15], V. Schönberg[5], T. Schörner-Sadenius[15], J. Schwartz[31], F. Sciulli[11], L.M. Shcheglova[34], R. Shehzadi[5], S. Shimizu[47,n], I. Singh[7,c], I.O. Skillicorn[20], W. Słomiński[14,g], W.H. Smith[56], V. Sola[22], A. Solano[49], D. Son[28], V. Sosnovtsev[33], A. Spiridonov[15,q], H. Stadie[22], L. Stanco[39], N. Stefaniuk[27], A. Stern[45], T.P. Stewart[51], A. Stifutkin[33], P. Stopa[12], S. Suchkov[33], G. Susinno[8], L. Suszycki[13], J. Sztuk-

Dambietz[22], D. Szuba[22], J. Szuba[15,r], A.D. Tapper[23], E. Tassi[8,d], J. Terrón[30], T. Theedt[15], H. Tiecke[36], K. Tokushuku[24,x], J. Tomaszewska[15,s], V. Trusov[27], T. Tsurugai[32], M. Turcato[22], O. Turkot[27,ab], T. Tymieniecka[54,ao], M. Vázquez[36,n], A. Verbytskyi[15], O. Viazlo[27], N.N. Vlasov[19,v], R. Walczak[38], W.A.T. Wan Abdullah[10], J.J. Whitmore[41,ag], K. Wichmann[15], L. Wiggers[36], M. Wing[52], M. Wlasenko[5], G. Wolf[15], H. Wolfe[56], K. Wrona[15], A.G. Yagües-Molina[15], S. Yamada[24], Y. Yamazaki[24,y], R. Yoshida[1], C. Youngman[15], O. Zabiegalov[27,ab], A.F. Żarnecki[53], L. Zawiejski[12], O. Zenaiev[15], W. Zeuner[15,n], B.O. Zhautykov[25], N. Zhmak[26,z], A. Zichichi[4], Z. Zolkapli[10], D.S. Zotkin[34]

[1] *Argonne National Laboratory, Argonne, Illinois 60439-4815, USA* [A]
[2] *Andrews University, Berrien Springs, Michigan 49104-0380, USA*
[3] *INFN Bologna, Bologna, Italy* [B]
[4] *University and INFN Bologna, Bologna, Italy* [B]
[5] *Physikalisches Institut der Universität Bonn, Bonn, Germany* [C]
[6] *H.H. Wills Physics Laboratory, University of Bristol, Bristol, United Kingdom* [D]
[7] *Panjab University, Department of Physics, Chandigarh, India*
[8] *Calabria University, Physics Department and INFN, Cosenza, Italy* [B]
[9] *Institute for Universe and Elementary Particles, Chonnam National University, Kwangju, South Korea*
[10] *Jabatan Fizik, Universiti Malaya, 50603 Kuala Lumpur, Malaysia* [E]
[11] *Nevis Laboratories, Columbia University, Irvington on Hudson, New York 10027, USA* [F]
[12] *The Henryk Niewodniczanski Institute of Nuclear Physics, Polish Academy of Sciences, Krakow, Poland* [G]
[13] *AGH-University of Science and Technology, Faculty of Physics and Applied Computer Science, Krakow, Poland* [H]
[14] *Department of Physics, Jagellonian University, Cracow, Poland*
[15] *Deutsches Elektronen-Synchrotron DESY, Hamburg, Germany*
[16] *Deutsches Elektronen-Synchrotron DESY, Zeuthen, Germany*
[17] *INFN Florence, Florence, Italy* [B]
[18] *University and INFN Florence, Florence, Italy* [B]
[19] *Fakultät für Physik der Universität Freiburg i.Br., Freiburg i.Br., Germany*
[20] *School of Physics and Astronomy, University of Glasgow, Glasgow, United Kingdom* [D]
[21] *Department of Engineering in Management and Finance, Univ. of the Aegean, Chios, Greece*
[22] *Hamburg University, Institute of Experimental Physics, Hamburg, Germany* [I]
[23] *Imperial College London, High Energy Nuclear Physics Group, London, United Kingdom* [D]
[24] *Institute of Particle and Nuclear Studies, KEK, Tsukuba, Japan* [J]
[25] *Institute of Physics and Technology of Ministry of Education and Science of Kazakhstan, Almaty, Kazakhstan*
[26] *Institute for Nuclear Research, National Academy of Sciences, Kyiv, Ukraine*
[27] *Department of Nuclear Physics, National Taras Shevchenko University of Kyiv, Kyiv, Ukraine*
[28] *Kyungpook National University, Center for High Energy Physics, Daegu, South Korea* [K]
[29] *Institut de Physique Nucléaire, Université Catholique de Louvain, Louvain-la-Neuve, Belgium* [L]
[30] *Departamento de Física Teórica, Universidad Autónoma de Madrid, Madrid, Spain* [M]
[31] *Department of Physics, McGill University, Montréal, Québec, Canada H3A 2T8* [N]
[32] *Meiji Gakuin University, Faculty of General Education, Yokohama, Japan* [J]

[33] *Moscow Engineering Physics Institute, Moscow, Russia* [O]
[34] *Lomonosov Moscow State University, Skobeltsyn Institute of Nuclear Physics, Moscow, Russia* [P]
[35] *Max-Planck-Institut für Physik, München, Germany*
[36] *NIKHEF and University of Amsterdam, Amsterdam, Netherlands* [Q]
[37] *Physics Department, Ohio State University, Columbus, Ohio 43210, USA* [A]
[38] *Department of Physics, University of Oxford, Oxford, United Kingdom* [D]
[39] *INFN Padova, Padova, Italy* [B]
[40] *Dipartimento di Fisica dell' Università and INFN, Padova, Italy* [B]
[41] *Department of Physics, Pennsylvania State University, University Park, Pennsylvania 16802, USA* [F]
[42] *Polytechnic University, Tokyo, Japan* [J]
[43] *Dipartimento di Fisica, Università 'La Sapienza' and INFN, Rome, Italy* [B]
[44] *Rutherford Appleton Laboratory, Chilton, Didcot, Oxon, United Kingdom* [D]
[45] *Raymond and Beverly Sackler Faculty of Exact Sciences, School of Physics, Tel Aviv University, Tel Aviv, Israel* [R]
[46] *Department of Physics, Tokyo Institute of Technology, Tokyo, Japan* [J]
[47] *Department of Physics, University of Tokyo, Tokyo, Japan* [J]
[48] *Tokyo Metropolitan University, Department of Physics, Tokyo, Japan* [J]
[49] *Università di Torino and INFN, Torino, Italy* [B]
[50] *Università del Piemonte Orientale, Novara, and INFN, Torino, Italy* [B]
[51] *Department of Physics, University of Toronto, Toronto, Ontario, Canada M5S 1A7* [N]
[52] *Physics and Astronomy Department, University College London, London, United Kingdom* [D]
[53] *Faculty of Physics, University of Warsaw, Warsaw, Poland*
[54] *National Centre for Nuclear Research, Warsaw, Poland*
[55] *Department of Particle Physics and Astrophysics, Weizmann Institute, Rehovot, Israel*
[56] *Department of Physics, University of Wisconsin, Madison, Wisconsin 53706, USA* [A]
[57] *Department of Physics, York University, Ontario, Canada M3J 1P3* [N]

[A] supported by the US Department of Energy
[B] supported by the Italian National Institute for Nuclear Physics (INFN)
[C] supported by the German Federal Ministry for Education and Research (BMBF), under contract No. 05 H09PDF
[D] supported by the Science and Technology Facilities Council, UK
[E] supported by an FRGS grant from the Malaysian government
[F] supported by the US National Science Foundation. Any opinion, findings and conclusions or recommendations expressed in this material are those of the authors and do not necessarily reflect the views of the National Science Foundation.
[G] supported by the Polish Ministry of Science and Higher Education as a scientific project No. DPN/N188/DESY/2009
[H] supported by the Polish Ministry of Science and Higher Education and its grants for Scientific Research
[I] supported by the German Federal Ministry for Education and Research (BMBF), under contract No. 05h09GUF, and the SFB 676 of the Deutsche Forschungsgemeinschaft (DFG)
[J] supported by the Japanese Ministry of Education, Culture, Sports, Science and Technology (MEXT) and its grants for Scientific Research
[K] supported by the Korean Ministry of Education and Korea Science and Engineering Foundation
[L] supported by FNRS and its associated funds (IISN and FRIA) and by an Inter-University Attraction Poles Programme subsidised by the Belgian Federal Science Policy Office
[M] supported by the Spanish Ministry of Education and Science through funds provided by CICYT
[N] supported by the Natural Sciences and Engineering Research Council of Canada (NSERC)
[O] partially supported by the German Federal Ministry for Education and Research (BMBF)
[P] supported by RF Presidential grant N 4142.2010.2 for Leading Scientific Schools, by the Russian Ministry of Education and Science through its grant for Scientific Research on High Energy Physics and under contract No.02.740.11.0244
[Q] supported by the Netherlands Foundation for Research on Matter (FOM)
[R] supported by the Israel Science Foundation

[a] now at University of Salerno, Italy
[b] now at Queen Mary University of London, United Kingdom
[c] also funded by Max Planck Institute for Physics, Munich, Germany
[d] also Senior Alexander von Humboldt Research Fellow at Hamburg University, Institute of Experimental Physics, Hamburg, Germany
[e] also at Cracow University of Technology, Faculty of Physics, Mathemathics and Applied Computer Science, Poland
[f] supported by the research grant No. 1 P03B 04529 (2005-2008)
[g] supported by the Polish National Science Centre, project No. DEC-2011/01/BST2/03643
[h] now at Rockefeller University, New York, NY 10065, USA
[i] now at DESY group FS-CFEL-1
[j] now at Institute of High Energy Physics, Beijing, China
[k] now at DESY group FEB, Hamburg, Germany
[l] also at Moscow State University, Russia
[m] now at University of Liverpool, United Kingdom
[n] now at CERN, Geneva, Switzerland
[o] also affiliated with Universtiy College London, UK
[p] now at Goldman Sachs, London, UK
[q] also at Institute of Theoretical and Experimental Physics, Moscow, Russia
[r] also at FPACS, AGH-UST, Cracow, Poland
[s] partially supported by Warsaw University, Poland
[t] now at Istituto Nucleare di Fisica Nazionale (INFN), Pisa, Italy
[u] now at Haase Energie Technik AG, Neumünster, Germany
[v] now at Department of Physics, University of Bonn, Germany
[w] also affiliated with DESY, Germany
[x] also at University of Tokyo, Japan
[y] now at Kobe University, Japan
[z] supported by DESY, Germany
[†] deceased
[aa] member of National Technical University of Ukraine, Kyiv Polytechnic Institute, Kyiv, Ukraine
[ab] member of National University of Kyiv - Mohyla Academy, Kyiv, Ukraine
[ac] partly supported by the Russian Foundation for Basic Research, grant 11-02-91345-DFG_a
[ad] Alexander von Humboldt Professor; also at DESY and University of Oxford
[ae] STFC Advanced Fellow
[af] now at LNF, Frascati, Italy
[ag] This material was based on work supported by the National Science Foundation, while working at the Foundation.
[ah] also at Max Planck Institute for Physics, Munich, Germany, External Scientific Member
[ai] now at Tokyo Metropolitan University, Japan

[aj] now at Nihon Institute of Medical Science, Japan
[ak] now at Osaka University, Osaka, Japan
[al] also at Łódź University, Poland
[am] member of Łódź University, Poland
[an] now at Department of Physics, Stockholm University, Stockholm, Sweden
[ao] also at Cardinal Stefan Wyszyński University, Warsaw, Poland

1 Introduction

The production of the well-established ground-state charm mesons D and D^* has been extensively studied in ep collisions at HERA. The large charm production cross section at HERA makes it possible to also investigate the excited charm-meson states. In a previous ZEUS analysis [1], with an integrated luminosity of 126 pb^{-1}, the orbitally excited states $D_1(2420)^0$ with $J^P = 1^+$ and $D_2^*(2460)^0$ with $J^P = 2^+$ were studied in the decay modes[1] $D_1(2420)^0 \to D^*(2010)^+\pi^-$ and $D_2^*(2460)^0 \to D^*(2010)^+\pi^-$, $D^+\pi^-$. The width of the D_1^0 was found to be significantly above the 2008 world-average value [2]. A study of the helicity angular distribution of the $D_1(2420)^0$ gave results that were consistent with some S-wave admixture in the decay $D_1^0 \to D^{*+}\pi^-$, contrary to Heavy Quark Effective Theory (HQET) predictions [3, 4] and to previous experimental results [5] which had yielded a pure D-wave decay in this channel.

In this paper the analysis was repeated with an independent data sample of higher integrated luminosity. In addition the production of the charged excited charm mesons $D_1(2420)^+$ and $D_2^*(2460)^+$ was studied for the first time at HERA in the decay modes $D_1(2420)^+ \to D^*(2007)^0\pi^+$ and $D_2^*(2460)^+ \to D^*(2007)^0\pi^+$, $D^0\pi^+$. For both the neutral and charged excited charm mesons the study also includes a measurement of fragmentation fractions and ratios of the D_2^* branching fractions.

The analysis was performed using data taken from 2003 to 2007, when HERA collided electrons or positrons at 27.5 GeV with protons at 920 GeV. The data correspond to an integrated luminosity of 373 pb^{-1}. The upgraded ZEUS detector included a microvertex detector, allowing the measurement of the decay vertex of charm mesons. In particular, the signal-to-background ratio was significantly improved for the D^+ meson, which has the highest lifetime among the charm hadrons.

To maximise the statistics, both photoproduction and deep inelastic scattering events were used in this analysis. Events produced in the photoproduction regime contributed $70 - 80\%$ of the selected charm-meson samples.

2 Experimental set-up

A detailed description of the ZEUS detector can be found elsewhere [6]. A brief outline of the components that are most relevant for this analysis is given below.

In the kinematic range of the analysis, charged particles were tracked in the central tracking detector (CTD) [7] and the microvertex detector (MVD) [8]. These components

[1] The corresponding anti-particle decays were also measured. Hereafter, charge conjugation is implied.

operated in a magnetic field of 1.43 T provided by a thin superconducting solenoid. The CTD consisted of 72 cylindrical drift-chamber layers, organised in nine superlayers covering the polar-angle[2] region $15^\circ < \theta < 164^\circ$. The MVD silicon tracker consisted of a barrel (BMVD) and a forward (FMVD) section. The BMVD contained three layers and provided polar-angle coverage for tracks from 30° to 150°. The four-layer FMVD extended the polar-angle coverage in the forward region to 7°. After alignment, the single-hit resolution of the MVD was 24 μm. The transverse distance of closest approach (DCA) of tracks to the nominal vertex in the X–Y plane was measured to have a resolution, averaged over the azimuthal angle, of $(46 \oplus 122/p_T)$ μm, with p_T in GeV. For CTD-MVD tracks that pass through all nine CTD superlayers, the momentum resolution was $\sigma(p_T)/p_T = 0.0029p_T \oplus 0.0081 \oplus 0.0012/p_T$, with p_T in GeV.

The high-resolution uranium–scintillator calorimeter (CAL) [9] consisted of three parts: the forward (FCAL), the barrel (BCAL) and the rear (RCAL) calorimeters. Each part was subdivided transversely into towers and longitudinally into one electromagnetic section (EMC) and either one (in RCAL) or two (in BCAL and FCAL) hadronic sections (HAC). The smallest subdivision of the calorimeter was called a cell. The CAL energy resolutions, as measured under test-beam conditions, were $\sigma(E)/E = 0.18/\sqrt{E}$ for electrons and $\sigma(E)/E = 0.35/\sqrt{E}$ for hadrons, with E in GeV.

The luminosity was measured using the Bethe-Heitler reaction $ep \to e\gamma p$ by a detector which consisted of an independent lead–scintillator calorimeter [10] and a magnetic spectrometer [11] system.

3 Event simulation

Monte Carlo (MC) samples of charm and beauty events were produced with the Pythia 6.221 [12] and the Rapgap 3.000 [13] event generators. The generation included direct photon processes, in which the photon couples directly to a parton in the proton, and resolved photon processes, where the photon acts as a source of partons, one of which participates in the hard scattering process. The CTEQ5L [14] and the GRV LO [15] parametrisations were used for the proton and photon parton density functions, respectively. The charm- and beauty-quark masses were set to 1.5 GeV and 4.75 GeV, respectively. The masses and widths for charm mesons were set to the latest PDG [16] values.

[2] The ZEUS coordinate system is a right-handed Cartesian system, with the Z axis pointing in the nominal proton beam direction, referred to as the "forward direction", and the X axis pointing left towards the centre of HERA. The coordinate origin is at the centre of the CTD. The pseudorapidity is defined as $\eta = -\ln\left(\tan\frac{\theta}{2}\right)$, where the polar angle, θ, is measured with respect to the Z axis.

Events for all processes were generated in proportion to the respective MC cross sections. The Lund string model was used for hadronisation in PYTHIA and RAPGAP. The Bowler modification [17] of the Lund symmetric fragmentation function [18] was used for the charm- and beauty-quark fragmentation.

The PYTHIA and RAPGAP generators were tuned to describe the photoproduction and the deep inelastic scattering regimes, respectively [1]. Subsequently, the PYTHIA events, generated with $Q^2 < 1.5\,\mathrm{GeV}^2$, were combined with the RAPGAP events, generated with $Q^2 > 1.5\,\mathrm{GeV}^2$, where Q^2 is the exchanged-photon virtuality.

The generated events were passed through a full simulation of the detector using GEANT 3.13 [19] and processed with the same reconstruction program as used for the data.

4 Event selection and reconstruction of ground-state charm mesons

The ZEUS trigger chain had three levels [6,20,21]. The first- and second-level trigger used CAL and CTD data to select ep collisions and to reject beam-gas events. At the third-level trigger, the full event information was available. All relevant trigger chains were used for the data. Triggers that required the presence of a reconstructed $D^{*+} \to D^0\pi^+ \to (K^-\pi^+)\pi^+$ or $(K^-\pi^+\pi^-\pi^+)\pi^+$, $D^+ \to K^-\pi^+\pi^+$ or $D^0 \to K^-\pi^+$ candidate constituted a major fraction of the selected events. However, events missed by these triggers but selected with other trigger branches were also used in the analysis. Applying, in the MC, either no trigger selection cuts or requiring at least one trigger chain to be passed did not affect the final measurements.

To ensure high purity in the event sample, the Z position of the primary vertex, reconstructed from CTD and MVD tracks, had to be within $|Z_{\mathrm{vtx}}| < 30$ cm. All charm mesons were reconstructed with tracks measured in the CTD and MVD. All tracks were required to have a transverse momentum, p_T, above 0.1 GeV, to start not further out than the first CTD superlayer and to reach at least the third superlayer. The tracks were assigned either to the reconstructed primary vertex or to a secondary decay vertex associated with the weak decay of a charm meson, D^+ or D^0. To ensure the use of well reconstructed MVD tracks, all tracks associated with the secondary vertex were required to have at least two BMVD measurements in the X–Y plane and two in the Z direction.

The decay-length significance is a powerful tool for rejection of combinatorial background. It is defined as $S = l/\sigma_l$, where the decay length l is the distance in the transverse plane between the production point and the decay vertex of a candidate charm meson projected on its momentum direction and σ_l is the uncertainty of this quantity [22]. The

quantity S is positive when the angle between the particle momenta and the direction from primary to secondary vertex is less than $\pi/2$; it is negative otherwise. The S distribution is asymmetric around zero, with a stronger positive contribution coming mostly from the charm mesons. The contributions to negative S values are due to background and resolution effects.

The combinatorial background was suppressed by selecting events above a minimum value of the ratio $p_T(D)/E_\perp^{\theta>10^\circ}$, where D denotes D^{*+}, D^+ or D^0 and $E_\perp^{\theta>10^\circ}$ is the transverse energy measured using all CAL cells outside a cone of 10° around the forward direction. In addition, to reduce background, the dE/dx values measured in the CTD of track candidates originating from the D mesons were used. The parametrisation of the dE/dx expectation values and the χ^2 probabilities l_K and l_π of the kaon and pion hypotheses, respectively, were obtained as described in previous analyses [23, 24]. The cuts $l_K > 0.03$ and $l_\pi > 0.01$ were applied.

4.1 D^{*+} reconstruction

D^{*+} mesons were identified via the decay modes $D^{*+} \to D^0\pi_s^+ \to (K^-\pi^+)\pi_s^+$ and $D^{*+} \to D^0\pi_s^+ \to (K^-\pi^+\pi^-\pi^+)\pi_s^+$, where π_s is a low-momentum ("soft") pion due to the small mass difference between D^{*+} and D^0. Tracks were combined to form D^0 candidates by calculating the invariant-mass combinations $M(K\pi)$ or $M(K\pi\pi\pi)$ with total charge zero. D^{*+} candidates were formed by adding a soft pion, π_s, with opposite charge to that of the kaon. Combinatorial background was reduced by applying cuts as detailed in Table 1.

The mass differences $\Delta M = M(K\pi\pi_s) - M(K\pi)$ and $\Delta M = M(K\pi\pi\pi\pi_s) - M(K\pi\pi\pi)$ were calculated for the D^{*+} candidates that passed the cuts of Table 1. Figure 1 shows the ΔM distributions for these D^{*+} candidates. Clean peaks are seen at the nominal value of $M(D^{*+}) - M(D^0)$ [16].

The ΔM distributions were fitted to a sum of a background function and a modified Gaussian function [1]. The fit yielded D^{*+} signals of 64988 ± 430 candidates for $D^0 \to K\pi$ and 24441 ± 310 candidates for $D^0 \to K\pi\pi\pi$. The fitted mass differences were 145.400 ± 0.003 MeV and 145.420 ± 0.003 MeV respectively, in agreement with the PDG average value [16]. Only D^{*+} candidates with $0.144 < \Delta M < 0.147$ GeV were used for the excited charm mesons analysis.

4.2 D^+ reconstruction

D^+ mesons were reconstructed from the decay $D^+ \to K^-\pi^+\pi^+$ with looser kinematic cuts than in the previous analysis [1], made possible by the cleaner identification with

the MVD. For each event, track pairs with equal charge and pion mass assignment were combined with a track with opposite charge with a kaon mass assignment to form a D^+ candidate. These tracks were refitted to a common decay vertex, and the invariant mass, $M(K\pi\pi)$, was calculated. The K and π tracks were required to have transverse momentum $p_T^K > 0.5$ GeV and $p_T^\pi > 0.35$ GeV and the distance of closest approach between each pair of the three tracks was required to be less than 0.3 cm. To suppress combinatorial background, the following cuts were applied:

- $\cos\theta^*(K) > -0.75$, where $\theta^*(K)$ is the angle between the kaon in the $K\pi\pi$ rest frame and the $K\pi\pi$ line of flight in the laboratory frame;
- the χ^2 of the fit of the decay vertex was less than 10;
- the decay-length significance, $S(D^+)$, was greater than 3.

Background from D^{*+} decays was removed by requiring $M(K\pi\pi) - M(K\pi) > 0.15$ GeV. Background from $D_s^+ \to \phi\pi,\ \phi \to K^+K^-$ was suppressed by requiring that the invariant mass of any two D^+ decay candidate tracks with opposite charge should be outside ± 8 MeV around the nominal ϕ mass when the kaon mass was assigned to both tracks. D^+ candidates in the kinematic range $p_T(D^+) > 2.8$ GeV and $|\eta(D^+)| < 1.6$ were kept for further analysis.

Figure 2 (a) shows the $M(K^-\pi^+\pi^+)$ distribution for D^+ candidates after the cuts. A clear signal is seen at the nominal value of the D^+ mass [16]. The mass distribution was fitted to a sum of a modified Gaussian function and a polynomial background. The fit yielded a D^+ signal of 39283 ± 452 events and a D^+ mass of 1869.1 ± 0.1 MeV, in agreement with the PDG average value [16]. Only D^+ candidates with $1.85 < M(K\pi\pi) < 1.89$ GeV were used for the excited charm mesons analysis.

4.3 D^0 reconstruction

D^0 mesons were reconstructed from the decay $D^0 \to K^-\pi^+$. For each event, two tracks with opposite charge and K and π mass assignments, respectively, were combined to form a D^0 candidate. These tracks were refitted to a common decay vertex, and the invariant mass, $M(K\pi)$, was calculated. Both tracks were required to have transverse momentum $p_T^K > 0.5$ GeV and $p_T^\pi > 0.7$ GeV and the distance of closest approach between these tracks was required to be less than 0.1 cm. To suppress combinatorial background, the following cuts were applied:

- $|\cos\theta^*(K)| < 0.85$, where $\theta^*(K)$ is the angle between the kaon in the $K\pi$ rest frame and the $K\pi$ line of flight in the laboratory frame;
- the χ^2 of the decay vertex was less than 20;

- the decay-length significance, $S(D^0)$, was bigger than 0.

D^0 candidates in the kinematic range $p_T(D^0) > 2.6$ GeV and $|\eta(D^0)| < 1.6$ were kept for further analysis.

Figure 2 (b) shows the $M(K^-\pi^+)$ distribution for D^0 candidates after the cuts. A clear signal is seen at the nominal value of the D^0 mass [16]. The mass distribution was fitted to a sum of a modified Gaussian function, a broad modified Gaussian representing the reflection produced by D^0 mesons with the wrong (opposite) kaon and pion mass assignment and a polynomial background. For the reflection, the shape parameters of the broad modified Gaussian were obtained from a study of the MC signal sample and the normalisation (integral) was set equal to that of the other modified Gaussian. The fit yielded a D^0 signal of 145740 ± 2944 events and a D^0 mass of 1864.1 ± 0.1 MeV which is 0.8 MeV lower than the PDG average value [16]. This deviation does not affect any of the results of the excited charm mesons. Only D^0 candidates with $1.845 < M(K\pi\pi) < 1.885$ GeV were used for the excited charm mesons analysis.

5 D_1 and D_2^* reconstruction

5.1 Reconstruction of the $D_1(2420)^0$ and $D_2^*(2460)^0$ mesons

The $D_1(2420)^0$ and $D_2^*(2460)^0$ mesons were reconstructed in the decay mode $D^{*+}\pi^-$ by combining each D^{*+} candidate with an additional track, assumed to be a pion (π_a), with a charge opposite to that of the D^*. Combinatorial background was reduced by applying the following cuts:

- $p_T(\pi_a) > 0.15$ GeV;
- $\eta(\pi_a) < 1.1$;
- $p_T(D^{*+}\pi_a)/E_\perp^{\theta>10^\circ} > 0.25$ (0.30) for the $D^0 \to K\pi$ ($D^0 \to K\pi\pi\pi$) channel;
- $\cos\theta^*(D^{*+}) < 0.9$, where $\theta^*(D^{*+})$ is the angle between the D^{*+} in the $D^{*+}\pi_a$ rest frame and the $D^{*+}\pi_a$ line of flight in the laboratory frame;
- the cut $l_\pi > 0.01$ was applied for π_a.

For each excited charm-meson candidate, the "extended" mass difference, $\Delta M^{\rm ext} = M(K\pi\pi_s\pi_a) - M(K\pi\pi_s)$ or $\Delta M^{\rm ext} = M(K\pi\pi\pi\pi_s\pi_a) - M(K\pi\pi\pi\pi_s)$, was calculated. Figure 3 (a) shows the invariant mass $M(D^{*+}\pi_a) = \Delta M^{\rm ext} + M(D^{*+}_{\rm PDG})$, where $M(D^{*+}_{\rm PDG})$ is the nominal D^{*+} mass [16]. A clear signal in the D_1^0/D_2^{*0} mass region is seen.

The $D_2^*(2460)^0$ was also reconstructed in the decay mode $D_2^*(2460)^0 \to D^+\pi^-$ by combining each D^+ candidate with an additional track, assumed to be a pion π_a, with a

charge opposite to that of the D^+. Combinatorial background was reduced by applying the following cuts:

- $p_T(\pi_a) > 0.3$ GeV;
- $\eta(\pi_a) < 1.5$;
- $p_T(D^+\pi_a)/E_\perp^{\theta>10^\circ} > 0.35$;
- $\cos\theta^*(D^+) < 0.8$, where $\theta^*(D^+)$ is the angle between the D^+ in the $D^+\pi_a$ rest frame and the $D^+\pi_a$ line of flight in the laboratory frame;
- the cut $l_\pi > 0.01$ was applied for π_a.

The $D_2^*(2460)^0 \to D^+\pi^-$ decay mode was reconstructed by calculating the "extended" mass difference $\Delta M^{\rm ext} = M(K\pi\pi\pi_a) - M(K\pi\pi)$. Figure 3 (b) shows the invariant mass $M(D^+\pi_a) = \Delta M^{\rm ext} + M(D^+_{\rm PDG})$, where $M(D^+_{\rm PDG})$ is the nominal D^+ mass [16]. A clear D_2^{*0} signal is seen. No indication of the $D_1^0 \to D^+\pi^-$ decay is seen, as expected from angular momentum and parity conservation for a $J^P = 1^+$ state. The various contributions to the mass spectrum will be discussed below.

5.2 Reconstruction of the $D_1(2420)^+$ and $D_2^*(2460)^+$ mesons

The charged excited meson $D_1(2420)^+$ has been seen [16] in the decay modes $D^{*0}\pi^+$ and $D^+\pi^+\pi^-$ and the charged excited meson $D_2^*(2460)^+$ has been seen [16] in the decay modes $D^{*0}\pi^+$ and $D^0\pi^+$. A search for D_1^+ and D_2^{*+} signals was performed in the mass distribution $M(D^0\pi^+)$. For the D_1^+ a possible $D^0\pi^+$ signal can arise only via a feed-down contribution (see Section 6). Each D^0 candidate was combined with an additional track, assumed to be a pion (π_a), with either positive or negative charge. Combinatorial background was reduced by applying the following cuts:

- $p_T(\pi_a) > 0.35$ GeV;
- $\eta(\pi_a) < 1.6$;
- $p_T(D^0\pi_a)/E_\perp^{\theta>10^\circ} > 0.3$;
- $\cos\theta^*(D^0) < 0.85$, where $\theta^*(D^0)$ is the angle between the D^0 in the $D^0\pi_a$ rest frame and the $D^0\pi_a$ line of flight in the laboratory frame;
- the cut $l_\pi > 0.01$ was applied for π_a.

For each excited charm-meson candidate, the "extended" mass difference $\Delta M^{\rm ext} = M(K\pi\pi_a) - M(K\pi)$ was calculated. Figure 4 shows the invariant mass $M(D^0\pi_a) = \Delta M^{\rm ext} + M(D^0_{\rm PDG})$, where $M(D^0_{\rm PDG})$ is the nominal D^0 mass [16]. A clear signal of $D_2^{*+} \to D^0\pi^+$ is seen. An enhancement above background is also seen at the mass region around 2.3 GeV. The various contributions to the mass spectrum will be discussed below.

6 Mass, width and helicity parameters of D_1 and D_2^*

A significant enhancement above background is seen in the $D^0\pi^+$ mass distribution (Fig. 4) around 2.3 GeV. A small excess of events is also seen in the same mass region in the $D^+\pi^-$ mass distribution (Fig. 3(b)).

The origin of these structures in both spectra is similar. They originate from the decay chains $D_1^0, D_2^{*0} \to D^{*+}\pi^-$, $D^{*+} \to D^+\pi^0$ and $D_1^+, D_2^{*+} \to D^{*0}\pi^+, D^{*0} \to D^0\pi^0$ or $D^{*0} \to D^0\gamma$. The π^0/γ are not seen in the tracking detectors; thus, the reconstruction is incomplete. However, since the available phase space in the $D^* \to D\pi^0$ decay is small and D is much heavier than π^0, the energy and momentum of D are close to those of D^*. Consequently, the enhancements in the $M(D^+\pi_a)$ (Fig. 3(b)) and $M(D^0\pi_a)$ (Fig. 4) distributions are feed-downs of the excited charm mesons D_1, D_2^*, shifted down approximately by the value of the π^0 mass, as verified by MC simulations.

6.1 Fitting procedure for D_1^0 and D_2^{*0}

To distinguish between $D_1^0, D_2^{*0} \to D^{*+}\pi^-$, their helicity angular distributions were used. These can be parametrised as $dN/d\cos\alpha \ \propto 1 + h\cos^2\alpha$, where α is the angle between the π_a and π_s momenta in the D^{*+} rest frame and h is the helicity parameter, predicted [3,4] to be $h = 3$ for D_1^0 and $h = -1$ for D_2^{*0}. Figure 5 shows the $M(D^{*+}\pi_a)$ distribution in four helicity bins. As expected from the above h values, the D_1^0 contribution increases with $|\cos\alpha|$ and dominates for $|\cos\alpha| > 0.75$, where the D_2^{*0} contribution is negligible.

A χ^2 fit was performed using simultaneously the $M(D^+\pi_a)$ distribution (Fig. 3(b)) and the $M(D^{*+}\pi_a)$ distributions in four helicity bins (Fig. 5). The background was described by four parameters a, b, c, d, separately for $M(D^{*+}\pi_a)$ and $M(D^+\pi_a)$, as $B(x) = ax^b \exp(-cx - dx^2)$, where $x = \Delta M^{\rm ext} - M_{\pi^+}$. Each resonance was fitted to a relativistic D-wave Breit-Wigner (BW) function [1] convoluted with a Gaussian resolution function with a width fixed to the corresponding MC prediction. Yields of the three signals, the D_1^0 and D_2^{*0} masses and widths and the D_1^0 helicity parameter, $h(D_1^0)$, were free parameters of the fit while $h(D_2^{*0})$ was fixed to the theoretical prediction [3,4], $h(D_2^{*0}) = -1$. Another free fit parameter was the contribution of the D_1^0, D_2^{*0} feed-downs to the $M(D^+\pi_a)$ distribution (see Appendix). The total normalisation of the sum of the feed-down processes from D_2^{*0} and D_1^0 decays was fitted relative to the direct signal peak yield from D_2^{*0} decay. The relative yields of the two feed-down contributions were taken to be equal to those for the direct signals in the $D^{*+}\pi^-$ decay channel.

The wide excited charm states [16] $D_1(2430)^0$ and $D_0^*(2400)^0$ are expected to contribute to the $M(D^{*+}\pi_a)$ and $M(D^+\pi_a)$ distributions, respectively. Even though these states are

hardly distinguishable from background due to their large width, they were included in the simultaneous fit with shapes described as relativistic S-wave BW functions [1]. Their masses and widths were set to the PDG values [16]. The yield of the $D_1(2430)^0$ was set to that of the narrow $D_1(2420)^0$ meson since both have the same spin-parity $J^P = 1^+$. The ratio of $D_0^*(2400)^0$ to the narrow state $D_2^*(2460)^0$ was a free parameter in the fit.

The results of the simultaneous fit are given in Table 2 and shown in Figs. 3 and 5. Systematic uncertainties are discussed in Section 8. All results from the new analysis (HERA II) are consistent with those from the previous ZEUS publication [1] (HERA I). The masses of both D_1^0 and D_2^{*0} are consistent with the PDG values [16] and with a recent BABAR measurement [25]. The D_1^0 width, $\Gamma(D_1^0) = 38.8 \pm 5.0(\text{stat.})^{+1.9}_{-5.4}(\text{syst.})$ MeV, is also consistent with the PDG value [16] of 27.1 ± 2.7 MeV, and is in good agreement with the BABAR measurement [25] of $31.4 \pm 0.5 \pm 1.3$ MeV. The D_2^{*0} width, $\Gamma(D_2^{*0}) = 46.6 \pm 8.1(\text{stat.})^{+5.9}_{-3.8}(\text{syst.})$ MeV, is consistent with the PDG value [16] of 49.0 ± 1.4 MeV, and with the BABAR measurement of $50.5 \pm 0.6 \pm 0.7$ MeV.

The D_1^0 helicity parameter, $h(D_1^0) = 7.8^{+6.7}_{-2.7}(\text{stat.})^{+4.6}_{-1.8}(\text{syst.})$, is consistent with the BABAR value of $h(D_1^0) = 5.72 \pm 0.25$ and somewhat above the theoretical prediction of $h = 3$ and measurements by CLEO [26] with $h(D_1^0) = 2.74^{+1.40}_{-0.93}$. The simultaneous fit with $h(D_1^0)$ fixed to the theoretical prediction, $h(D_1^0) = 3$, yielded masses and widths of D_2^{*0} and D_1^0 that are somewhat away from the PDG values [16]. Repeating the simultaneous fit with $h(D_2^{*0})$ as a free parameter yielded similar results for all other free parameters with somewhat larger errors and with $h(D_2^{*0}) = -1.16 \pm 0.35$, in good agreement with the theoretical prediction of $h = -1$.

The helicity angular distribution for a $J^P = 1^+$ state with a mixture of D- and S-wave is

$$\frac{dN}{d\cos\alpha} \propto r + (1-r)(1+3\cos^2\alpha)/2 + \sqrt{2r(1-r)}\cos\phi(1-3\cos^2\alpha), \qquad (1)$$

where $r = \Gamma_S/(\Gamma_S + \Gamma_D)$, $\Gamma_S(\Gamma_D)$ is the $S(D)$-wave partial width and ϕ is relative phase between the two amplitudes. The relation between h, r and ϕ is given by

$$\cos\phi = \frac{(3-h)/(3+h) - r}{2\sqrt{2r(1-r)}}. \qquad (2)$$

The range of the measured $h(D_1^0)$ restricted to one standard deviation is shown in Fig. 6 in a plot of $\cos\phi$ versus r. This range is consistent with the BABAR measurement [25]. The range restricted by CLEO [26] is outside the range of this measurement and that of BABAR. A similar measurement by the BELLE collaboration [5] is consistent with a pure D-wave, i.e. $\Gamma_S/(\Gamma_S + \Gamma_D) = 0$.

In a recent paper [25] the BABAR Collaboration searched for excited D meson states in $e^+e^- \to c\bar{c} \to D^{(*)}\pi + X$ with very large statistics. In addition to the D_1^0 and D_2^{*0}

resonances, they saw two new structures near 2.6 GeV in the $D^+\pi^-$ and $D^{*+}\pi^-$ mass distributions, $D(2550)^0$ and $D^*(2600)^0$, and interpreted them as being radial excitations of the well-known D^0 and D^{*0}, respectively. A small enhancement of events above the solid curve in the region near 2.6 GeV is seen in the $M(D^{*+}\pi^-)$ distribution (Figs. 3(a),5). Adding the new BABAR states to the fit gave insignificant yields of the states and did not significantly change the results of the other fit parameters.

6.2 Fitting procedure for D_1^+ and D_2^{*+}

To extract the D_1^+ and D_2^{*+} masses and yields, a minimal χ^2 fit was performed using the $M(D^0\pi_a)$ distribution (Fig. 4). Both resonances were fitted to relativistic D-wave Breit-Wigner (BW) functions [1] convoluted with a Gaussian resolution function with a width fixed to the corresponding MC prediction. Yields of the $D_2^{*+} \to D^0\pi^+$ and the two feed-downs $D_1^+, D_2^{*+} \to D^{*0}\pi^+$ (see Appendix) and the D_1^+ and D_2^{*+} masses were free parameters of the fit. The D_1^+ and D_2^{*+} widths were fixed to the PDG values [16] and the D_1^+ and D_2^{*+} helicities were fixed to the theoretical prediction [3, 4], $h(D_1^+) = 3$ and $h(D_2^{*+}) = -1$. The background was parametrised with four parameters a, b, c, d as $B(x) = ax^b \exp(-cx - dx^2)$, where $x = \Delta M^{\text{ext}} - M_{\pi^+}$.

The results of the fit (yields and masses) are given in Table 3 and shown in Fig. 4. The masses of D_1^+ and D_2^{*+} are consistent with the PDG values [16]. The D_2^{*+} mass is also consistent with the BABAR measurement [25].

7 D_2^* decay branching ratios and D_1/D_2^* fragmentation fractions

7.1 The neutral excited mesons

The branching ratio for D_2^{*0} and the fragmentation fractions for D_1^0 and D_2^{*0} were measured using the channels $D_2^{*0} \to D^+\pi^-$ and $D_1^0, D_2^{*0} \to D^{*+}\pi^-$ with $D^{*+} \to D^0\pi_s^+ \to (K^-\pi^+)\pi_s^+$. The numbers of reconstructed $D_1^0, D_2^{*0} \to D^{*+}\pi^-$ and $D_2^{*0} \to D^+\pi^-$ decays were divided by the numbers of reconstructed D^{*+} and D^+ mesons, yielding the fractions of D^{*+} and D^+ mesons originating from the D_1^0 and D_2^{*0} decays. To correct the measured fractions for detector effects, ratios of acceptances were calculated using the MC simulation for the $D_1^0, D_2^{*0} \to D^{*+}\pi^-$ and $D_2^{*0} \to D^+\pi^-$ states to the inclusive D^{*+} and D^+ acceptances, respectively.

Beauty production at HERA is smaller than charm production by two orders of magnitude. A subtraction of the b-quark relative contribution in a previous ZEUS analysis [1]

changed the relative acceptances by less than 1.5% of their values. Consequently, no such subtraction was performed in this analysis and the MC simulation included the beauty production processes. A variation of this contribution was considered for the systematics (Section 8).

The fractions, $\mathcal{F}$, of D^{*+} mesons originating from D_1^0 and D_2^{*0} decays were calculated in the kinematic range $|\eta(D^{*+})| < 1.6$ and $p_T(D^{*+}) > 1.5\,\text{GeV}$ for the D^{*+} decay and the fraction of D^+ mesons originating from D_2^{*0} decays was calculated in the kinematic range $p_T(D^+) > 2.8\,\text{GeV}$ and $|\eta(D^+)| < 1.6$.

The fractions measured in the restricted $p_T(D^{*+}, D^+)$ and $\eta(D^{*+}, D^+)$ kinematic ranges were extrapolated to the fractions in the full kinematic phase space using the Bowler modification [17] of the Lund symmetric fragmentation function [18] as implemented in PYTHIA [27]. Applying the estimated extrapolation factors, ~ 1.12 for $\mathcal{F}_{D_1^0\to D^{*+}\pi^-/D^{*+}}$, ~ 1.16 for $\mathcal{F}_{D_2^{*0}\to D^{*+}\pi^-/D^{*+}}$ and ~ 1.34 for $\mathcal{F}_{D_2^{*0}\to D^{+}\pi^-/D^{+}}$, gives

$$\mathcal{F}^{\text{extr}}_{D_1^0\to D^{*+}\pi^-/D^{*+}} = 8.5 \pm 1.4(\text{stat.})^{+1.2}_{-1.6}(\text{syst.})\,\%, \tag{3}$$

$$\mathcal{F}^{\text{extr}}_{D_2^{*0}\to D^{*+}\pi^-/D^{*+}} = 4.7 \pm 1.3(\text{stat.})^{+1.2}_{-0.8}(\text{syst.})\,\%, \tag{4}$$

$$\mathcal{F}^{\text{extr}}_{D_2^{*0}\to D^{+}\pi^-/D^{+}} = 6.7 \pm 2.4(\text{stat.})^{+1.5}_{-1.1}(\text{syst.})\,\%. \tag{5}$$

In the full kinematic phase space, the extrapolated fractions of D^{*+} originating from D_1^0 and D_2^{*0} and of D^+ originating from D_2^{*0} can be expressed [1] in terms of the rates of c-quarks hadronising to a given charm meson ("fragmentation fractions"), $f(c\to D_1^0)$, $f(c\to D_2^{*0})$, $f(c\to D^{*+})$ and $f(c\to D^+)$ and the corresponding branching fractions $\mathcal{B}_{D_1^0\to D^{*+}\pi^-}$, $\mathcal{B}_{D_2^{*0}\to D^{*+}\pi^-}$ and $\mathcal{B}_{D_2^{*0}\to D^{+}\pi^-}$.

From the expressions used in a previous ZEUS publication [1], the fragmentation fractions $f(c\to D_1^0)$ and $f(c\to D_2^{*0})$ and the ratio of the two branching fractions for the D_2^{*0} meson can be shown to be:

$$f(c\to D_1^0) = \frac{\mathcal{F}^{\text{extr}}_{D_1^0\to D^{*+}\pi^-/D^{*+}}}{\mathcal{B}_{D_1^0\to D^{*+}\pi^-}} f(c\to D^{*+}), \tag{6}$$

$$f(c\to D_2^{*0}) = \frac{\mathcal{F}^{\text{extr}}_{D_2^{*0}\to D^{*+}\pi^-/D^{*+}} f(c\to D^{*+}) + \mathcal{F}^{\text{extr}}_{D_2^{*0}\to D^{+}\pi^-/D^{+}} f(c\to D^{+})}{\mathcal{B}_{D_2^{*0}\to D^{*+}\pi^-} + \mathcal{B}_{D_2^{*0}\to D^{+}\pi^-}}, \tag{7}$$

$$\frac{\mathcal{B}_{D_2^{*0}\to D^{+}\pi^-}}{\mathcal{B}_{D_2^{*0}\to D^{*+}\pi^-}} = \frac{\mathcal{F}^{\text{extr}}_{D_2^{*0}\to D^{+}\pi^-/D^{+}} f(c\to D^{+})}{\mathcal{F}^{\text{extr}}_{D_2^{*0}\to D^{*+}\pi^-/D^{*+}} f(c\to D^{*+})}\,. \tag{8}$$

The $f(c \to D^{*+})$ and $f(c \to D^{+})$ values used were obtained as a combination of data from HERA and e^+e^- colliders [28]:

$$f(c \to D^{*+}) = 22.87 \pm 0.56(\text{stat.} \oplus \text{syst.})^{+0.45}_{-0.56}(\text{br.})\,\%,$$

$$f(c \to D^{+}) = 22.56 \pm 0.77(\text{stat.} \oplus \text{syst.}) \pm 1.00(\text{br.})\,\%.$$

where the third uncertainties are due to the branching-ratio uncertainties.

Taking into account the correlations in the simultaneous fit performed to obtain the values in Eqs. (4) and (5) yields

$$\frac{\mathcal{B}_{D_2^{*0}\to D^+\pi^-}}{\mathcal{B}_{D_2^{*0}\to D^{*+}\pi^-}} = 1.4 \pm 0.3(\text{stat.}) \pm 0.3(\text{syst.}),$$

in good agreement with the PDG world-average value 1.56 ± 0.16 [16]. Theoretical models [29–31] predict the ratio to be in the range from 1.5 to 3.

Neglecting the contributions of the non-dominant decay mode $D_1^0 \to D^0\pi^+\pi^-$ [16] and assuming isospin conservation, for which

$$\mathcal{B}_{D_1^0\to D^{*+}\pi^-} = 2/3, \quad \mathcal{B}_{D_2^{*0}\to D^{*+}\pi^-} + \mathcal{B}_{D_2^{*0}\to D^{+}\pi^-} = 2/3,$$

and using Eqs. (6) and (7) yields

$$f(c \to D_1^0) = 2.9 \pm 0.5(\text{stat.}) \pm 0.5(\text{syst.})\,\%,$$

$$f(c \to D_2^{*0}) = 3.9 \pm 0.9(\text{stat.})^{+0.8}_{-0.6}(\text{syst.})\,\%.$$

The measured fragmentation fractions were found to be consistent with those obtained in e^+e^- annihilations [32]. The sum of the two fragmentation fractions,

$$f(c \to D_1^0) + f(c \to D_2^{*0}) = 6.8 \pm 1.0(\text{stat.})^{+0.9}_{-0.8}(\text{syst.})\,\%,$$

agrees with the prediction of the tunneling model of 8.5% [33].

Assuming uncorrelated errors, the ratio

$$f(c \to D_1^0)/f(c \to D_2^{*0}) = 0.8 \pm 0.2(\text{stat.}) \pm 0.2(\text{syst.})$$

is in good agreement with the simple spin-counting prediction of 3/5.

7.2 The charged excited mesons

The branching ratio for D_2^{*+} and the fragmentation fractions for D_1^+ and D_2^{*+} were measured using the channels $D_2^{*+} \to D^0\pi^+$ and $D_1^+, D_2^{*+} \to D^{*0}\pi^+$ with $D^{*0} \to D^0\pi^0/\gamma$, where the π^0/γ are not measured directly. Since D^{*0} decays always to D^0 [16], the number of D^{*0} and D^0 originating from D_1^+/D_2^{*+} are identical. The number of reconstructed $D_1^+/D_2^{*+} \to D^{*0}\pi^+; D^{*0} \to D^0\pi^0/\gamma$ and $D_2^{*+} \to D^0\pi^+$ decays were thus divided by the total number of reconstructed D^0 mesons, yielding the fractions of D^0 mesons originating from D_1^+/D_2^{*+} decays. Detector effects were corrected as described in Section 7.1. The above fractions were calculated in the kinematic range $p_T(D^0) > 2.6$ GeV and $|\eta(D^0)| < 1.6$ and extrapolated to the fractions in the full kinematic phase space as for the D_1^0 and D_2^{*0} (Section 7.1). Applying the extrapolation factors, ~ 1.28 for $D_1^+ \to D^{*0}\pi^+$, ~ 1.18 for $D_2^{*+} \to D^{*0}\pi^+$ and ~ 1.35 for $D_2^{*+} \to D^0\pi^+$ gives

$$\mathcal{F}^{\rm extr}_{D_1^+ \to D^{*0}\pi^+/D^0} = 5.4 \pm 2.1(\text{stat.})^{+2.3}_{-0.3}(\text{syst.})\,\%, \tag{9}$$

$$\mathcal{F}^{\rm extr}_{D_2^{*+} \to D^{*0}\pi^+/D^0} = 1.8 \pm 0.9(\text{stat.})^{+0.5}_{-0.3}(\text{syst.})\,\%, \tag{10}$$

$$\mathcal{F}^{\rm extr}_{D_2^{*+} \to D^0\pi^+/D^0} = 2.0 \pm 0.5(\text{stat.})^{+0.4}_{-0.2}(\text{syst.})\,\%. \tag{11}$$

The fractions of D^{*0}/D^0 mesons originating from D_1^+/D_2^{*+} decays can be expressed as

$$\mathcal{F}^{\rm extr}_{D_1^+ \to D^{*0}\pi^+/D^{*0}} \equiv \frac{N(D_1^+ \to D^{*0}\pi^+)}{N(D^{*0})} = \frac{f(c \to D_1^+)}{f(c \to D^{*0})}\mathcal{B}_{D_1^+ \to D^{*0}\pi^+}, \tag{12}$$

$$\mathcal{F}^{\rm extr}_{D_2^{*+} \to D^{*0}\pi^+/D^{*0}} \equiv \frac{N(D_2^{*+} \to D^{*0}\pi^+)}{N(D^{*0})} = \frac{f(c \to D_2^{*+})}{f(c \to D^{*0})}\mathcal{B}_{D_2^{*+} \to D^{*0}\pi^+}, \tag{13}$$

$$\mathcal{F}^{\rm extr}_{D_2^{*+} \to D^0\pi^+/D^0} \equiv \frac{N(D_2^{*+} \to D^0\pi^+)}{N(D^0)} = \frac{f(c \to D_2^{*+})}{f(c \to D^0)}\mathcal{B}_{D_2^{*+} \to D^0\pi^+}, \tag{14}$$

where N denotes the acceptance-corrected number of events.

The ratio of the fragmentation fractions $f(c \to D^{*0})$ and $f(c \to D^0)$ can be expressed as

$$\frac{f(c \to D^{*0})}{f(c \to D^0)} = \frac{N(D^{*0})}{N(D^0)}.$$

Consequently, Eqs. (12) and (13) can be written as

$$\frac{N(D_1^+ \to D^{*0}\pi^+)}{N(D^0)} = \frac{f(c \to D_1^+)}{f(c \to D^0)} \mathcal{B}_{D_1^+ \to D^{*0}\pi^+},$$

$$\frac{N(D_2^{*+} \to D^{*0}\pi^+)}{N(D^0)} = \frac{f(c \to D_2^{*+})}{f(c \to D^0)} \mathcal{B}_{D_2^{*+} \to D^{*0}\pi^+},$$

yielding

$$f(c \to D_1^+) = \frac{f(c \to D^0)}{N(D^0)} \frac{N(D_1^+ \to D^{*0}\pi^+)}{\mathcal{B}_{D_1^+ \to D^{*0}\pi^+}},$$

$$f(c \to D_2^{*+}) = \frac{f(c \to D^0)}{N(D^0)} \frac{N(D_2^{*+} \to D^{*0}\pi^+) + N(D_2^{*+} \to D^0\pi^+)}{\mathcal{B}_{D_2^{*+} \to D^{*0}\pi^+} + \mathcal{B}_{D_2^{*+} \to D^0\pi^+}},$$

$$\frac{\mathcal{B}_{D_2^{*+} \to D^0\pi^+}}{\mathcal{B}_{D_2^{*+} \to D^{*0}\pi^+}} = \frac{N(D_2^{*+} \to D^0\pi^+)}{N(D_2^{*+} \to D^{*0}\pi^+)} \ .$$

Neglecting the non-dominant decay mode $D_1^+ \to D^+\pi^+\pi^-$ [16], assuming isospin conservation, for which

$$\mathcal{B}_{D_1^+ \to D^{*0}\pi^+} = 2/3, \quad \mathcal{B}_{D_2^{*+} \to D^{*0}\pi^+} + \mathcal{B}_{D_2^{*+} \to D^0\pi^+} = 2/3,$$

and using Eqs. (9 – 11) and the fragmentation fraction [28]

$$f(c \to D^0) = 56.43 \pm 1.51(\text{stat.} \oplus \text{syst.})^{+1.35}_{-1.64}(\text{br.})\ \%,$$

gives

$$f(c \to D_1^+) = 4.6 \pm 1.8(\text{stat.})^{+2.0}_{-0.3}(\text{syst.})\ \%,$$

$$f(c \to D_2^{*+}) = 3.2 \pm 0.8(\text{stat.})^{+0.5}_{-0.2}(\text{syst.})\ \%,$$

$$f(c \to D_1^+) + f(c \to D_2^{*+}) = 7.8 \pm 2.0(\text{stat.})^{+2.0}_{-0.4}(\text{syst.})\ \%,$$

$$f(c \to D_1^+)/f(c \to D_2^{*+}) = 1.4 \pm 0.7(\text{stat.})^{+0.7}_{-0.1}(\text{syst.}),$$

in agreement with the fragmentation fractions of the neutral excited charm mesons (Section 7.1).

The ratio of the branching fractions of the two dominant decay modes of the D_2^{*+},

$$\frac{\mathcal{B}_{D_2^{*+}\to D^0\pi^+}}{\mathcal{B}_{D_2^{*+}\to D^{*0}\pi^+}} = 1.1 \pm 0.4(\text{stat.})^{+0.3}_{-0.2}(\text{syst.}), \tag{15}$$

significantly improves on the accuracy of the PDG [16] value of $1.9 \pm 1.1 \pm 0.3$. BABAR measured the ratio [34] $\frac{\mathcal{B}_{D_2^{*+}\to D^0\pi^+}}{\mathcal{B}_{D_2^{*+}\to D^0\pi^+}+\mathcal{B}_{D_2^{*+}\to D^{*0}\pi^+}} = 0.62 \pm 0.03 \pm 0.02$, which depends on some assumptions and is not included in the PDG averages [16]. Using the value given in Eq.(15) yields a ratio $\frac{\mathcal{B}_{D_2^{*+}\to D^0\pi^+}}{\mathcal{B}_{D_2^{*+}\to D^0\pi^+}+\mathcal{B}_{D_2^{*+}\to D^{*0}\pi^+}} = 0.52^{+0.08}_{-0.13}(\text{stat.}) \pm 0.05(\text{syst.})$, in good agreement with the BABAR result.

8 Systematic uncertainties

The systematic uncertainties were determined by appropriate variations of the analysis procedure, generally by the uncertainties in our knowledge of the variables considered, and repeating the calculation of the results. The following sources of uncertainty were considered:

- $\{\delta_1\}$ The stability of the fit results was checked by a variation of the selection cuts which are most sensitive to the ratio of signal and background in the data:
  - the cut on the minimal transverse momentum of the D^{*+}, D^+ and D^0 candidates was varied by $\pm 100\,\text{MeV}$;
  - the cut on the minimal transverse momentum of the extra pion in the excited D meson analysis was varied by $\pm 10\,\text{MeV}$;
  - the selection cut on the cosine of angle between extra pions and charged (neutral) excited D meson candidates was changed by ± 0.1 (± 0.05);
  - the widths of the mass windows used for the selection of D^{*+} and D^0 candidates in the excited charm meson analyses were varied by $\pm 5\%$ for each p_T dependent window (see Table 1), while for the D^+ candidates it was varied by $\pm 12.5\%$.
- $\{\delta_2\}$ The CAL energy scale is known with $\pm 2\%$ uncertainty and was varied accordingly in the simulation.
- $\{\delta_3\}$ The uncertainties related to the fit procedure were obtained as follows:
  - the ranges for the signal fits were reduced on either side by 16 MeV for the $D^{*+}\pi$ and $D^+\pi$ mass spectra and 24 MeV for the $D^0\pi$ mass spectrum;
  - the background shape was changed to that used by BABAR (Eq. 1 in ref. [25]);

- the widths of the Gaussians used to parametrise the mass resolutions were changed by $\pm 20\%$;
- all the masses and widths of wide states were set free in the fit. Since with the present data alone these parameters are not determined well, the world-average values from PDG [16] were used as additional constraints. This was implemented by adding for each parameter P (width or mass) a term $\frac{(P-P_{\rm PDG})^2}{\sigma(P_{\rm PDG})^2}$ to the χ^2-function. Here $P_{\rm PDG}$ and $\sigma(P_{\rm PDG})$ denote the parameter value and its uncertainty from PDG [16];
- the background functions in the four helicity intervals were allowed to have separate normalisations;
- the helicity parameter of the D_2^{*0} meson in the fit was set free (Section 5.1).

- $\{\delta_4\}$ The uncertainties of $M(D^{*+})_{\rm PDG}$, $M(D^0)_{\rm PDG}$, $M(D^+)_{\rm PDG}$ were taken into account.
- $\{\delta_5\}$ The widths of D_1^+ and D_2^{*+} were varied within their uncertainties taken from PDG [16].
- $\{\delta_6\}$ The uncertainty of the beauty contamination was determined by varying the beauty fraction in the MC sample between 0 and 200% of the reference amount.
- $\{\delta_7\}$ The extrapolation uncertainties were determined by varying relevant parameters of the PYTHIA simulation using the Bowler modification [17] of the Lund symmetric fragmentation function [18]. The following variations were performed:
  - the mass of the c quark was varied from its nominal value of 1.5 GeV by ± 0.2 GeV;
  - the strangeness suppression factor was varied from its nominal value of 0.3 by ± 0.1;
  - the fraction of the lowest-mass charm mesons produced in a vector state was varied from its nominal value of 0.6 by ± 0.1;
  - the Bowler fragmentation function parameter r_c was varied from the predicted value 1 to 0.5; the a and b parameters of the Lund symmetric function were varied by $\pm 20\%$ around their default values [27].

A possible model dependence of the acceptance corrections was checked by reweighting the D-meson transverse momentum distribution in the MC to match the distribution observed in the data; no significant effect on any result was found. As a further cross check the selected pseudorapidity range of the extra pion, which is not the same for the different decay channels (see Section 5), was varied, and again no significant effect on any result was observed. The uncertainties of the fragmentation fractions $f(c \to D^{*+})$, $f(c \to D^+)$ and $f(c \to D^0)$ were included by adding in quadrature their statistical and systematic

uncertainties and the uncertainties originating from the branching-ratio uncertainties. The resulting uncertainty is included in δ_7.

The contributions from all systematic uncertainties were calculated separately for positive and negative variations and added in quadrature. The obtained values are listed in Tables 4–7. There is no single dominating source of systematic uncertainty. The total systematic uncertainties are comparable to the statistical errors.

9 Summary

The full HERA data taken from 2003 to 2007 with an integrated luminosity of 373 pb^{-1} has been used to study the production of excited charm mesons. Signals of $D_1(2420)^0$ and $D_2^*(2460)^0$ were seen in the $D^{*+}\pi^-$ decay mode and a clear $D_2^*(2460)^0$ signal was seen in the $D^+\pi^-$ decay mode. The measured D_1^0 and D_2^{*0} masses and widths are in good agreement with the latest PDG values. The measured D_1^0 helicity parameter allows for some S-wave mixing in its decay to $D^{*+}\pi^-$. The result is also consistent with a pure D-wave hypothesis. The helicity of D_2^{*0}, when set free in the fit, is consistent with the HQET prediction, $h = -1$.

A clear $D_2^*(2460)^+$ signal is seen for the first time at HERA in the $D^0\pi^+$ decay mode. Feed-downs of both resonances $D_1(2420)^+$ and $D_2^*(2460)^+$ in the decay mode $D^{*0}\pi^+$ are seen in the expected mass region of $M(D^0\pi^+) \approx 2.3$ GeV. The measured D_1^+ and D_2^{*+} masses are in good agreement with the PDG values and the D_2^{*+} mass is consistent with the BABAR measurement.

The fractions of c-quarks hadronising into D_1^0 and D_2^{*0} are consistent with those from the previous ZEUS publication and with e^+e^- annihilation results, in agreement with charm fragmentation universality. The fractions of c-quarks hadronising into D_1^+ and D_2^{*+} were measured for the first time and are consistent, respectively, with the fractions of the neutral charm excited states D_1^0 and D_2^{*0}.

The ratios of the neutral and charged D_2^* branching ratios into $D\pi$ and $D^*\pi$ are consistent with the PDG values.

Acknowledgements

We appreciate the contributions to the construction and maintenance of the ZEUS detector of many people who are not listed as authors. The HERA machine group and the

DESY computing staff are especially acknowledged for their success in providing excellent operation of the collider and the data-analysis environment. We thank the DESY directorate for their strong support and encouragement.

10 Appendix: Parametrisation of the feed-down contributions

Let us consider the decay chain $D_{1,2} \to D^*\pi,\ D^* \to D\pi^0$ in the D^* centre-of-mass system. Here $D_{1,2}$ is a neutral (positively charged) excited charm meson D_1 or D_2^*, D^* is a positively charged (neutral) D^*, π is a negatively (positively) charged pion and D is a positively charged (neutral) D (charge conjugation is implied). In this system $D_{1,2}$ and π in the initial decay and D and π^0 in the subsequent decay are produced with back-to-back momenta. The momenta of particles in this system are:

$$P_\pi^2 = \left(\frac{M^2 - M_{D^*}^2 - M_\pi^2}{2M_{D^*}}\right)^2 - M_\pi^2,$$

where M is the $D_{1,2}$ mass;

$$P_D^2 = P_{\pi^0}^2 = \left(\frac{M_{D^*}^2 - M_D^2 + M_{\pi^0}^2}{2M_{D^*}}\right)^2 - M_{\pi^0}^2.$$

The measured $M(D\pi)$ is given by

$$M_m^2 = M^2(D\pi) = M_D^2 + M_\pi^2 + 2\sqrt{(P_D^2 + M_D^2)(P_\pi^2 + M_\pi^2)} - 2P_D P_\pi \cos\alpha,$$

where α is the helicity angle between π^0 and π. Using the equations above, M_m can be parametrised as:

$$M_m^2 = M^2(1-a) + b + g\sqrt{(M^2 - d_1)(M^2 - d_2)}\cos\alpha, \tag{16}$$

where

$$a = ({M_{D^*}}^2 + {M_{\pi^0}}^2 - {M_D}^2)/(2{M_{D^*}}^2),$$

$$b = {M_{\pi^0}}^2 - ({M_{D^*}}^2 - {M_\pi}^2)({M_{D^*}}^2 + {M_{\pi^0}}^2 - {M_D}^2)/(2{M_{D^*}}^2),$$

$$g = \sqrt{({M_{D^*}}^2 + {M_{\pi^0}}^2 - {M_D}^2)^2 - 4{M_{D^*}}^2{M_{\pi^0}}^2}/(2{M_{D^*}}^2),$$

$$d_1 = (M_{D^*} + M_\pi)^2,$$

$$d_2 = (M_{D^*} - M_\pi)^2.$$

From Eq.(16), M is obtained as a function of M_m and α

$$M = M(M_m, \alpha).$$

If the spectrum shape of M is

$$\frac{dN}{dM} = f(M),$$

where N is the number of candidates, then the M_m spectrum shape is

$$\frac{dN}{dM_m} = f(M(M_m))\frac{dM}{dM_m}.$$

Combining Eq.(16) with the normalised helicity angular distribution

$$\frac{dN}{d(\cos\alpha)} = \frac{1 + h\cos^2\alpha}{2(1 + h/3)},$$

yields

$$\frac{d^2N}{dM_m d(\cos\alpha)} = f(M(M_m, \alpha))\frac{dM}{dM_m}\frac{1 + h\cos^2\alpha}{2(1 + h/3)}.$$

The fit uses the integral over $\cos\alpha$

$$\frac{dN}{dM_m} = \int_{-1}^{1} f(M(M_m, \alpha))\frac{dM}{dM_m}\frac{1 + h\cos^2\alpha}{2(1 + h/3)}d(\cos\alpha). \tag{17}$$

Here $f(M)$ is parametrised by a relativistic Breit-Wigner function as for the prompt signals.

For the description of the $D^0\pi$ spectrum, the $D^{*0} \to D^0\gamma$ decay was also taken into account by replacing M_{π^0} with $M_\gamma = 0$ in the equations above. For the description of the $D^+\pi$ spectrum, the contribution of the $D^{*+} \to D^+\gamma$ decay was neglected [16].

References

[1] ZEUS Coll., S. Chekanov et al., Eur. Phys. J. **C 60**, 25 (2009).

[2] Particle Data Group, C. Amsler et al., Phys. Lett. **B 667**, 1 (2008).

[3] N. Isgur and M.B. Wise, Phys. Lett. **B 232**, 113 (1989).

[4] M. Neubert, Phys. Rev. **A 245**, 259 (1994).

[5] BELLE Coll., K. Abe et al., Phys. Rev. **D 69**, 112002 (2004).

[6] ZEUS Coll., U. Holm (ed.), *The ZEUS Detector*. Status Report (unpublished), DESY (1993), available on `http://www-zeus.desy.de/bluebook/bluebook.html`.

[7] N. Harnew et al., Nucl. Instrum. Meth. **A 279**, 290 (1989);
B. Foster et al., Nucl. Phys. Proc. Suppl. **B 32**, 181 (1993);
B. Foster et al., Nucl. Instrum. Meth. **A 338**, 254 (1994).

[8] A. Polini et al., Nucl. Instrum. Meth. **A 581**, 656 (2007).

[9] M. Derrick et al., Nucl. Instrum. Meth. **A 309**, 77 (1991);
A. Andresen et al., Nucl. Instrum. Meth. **A 309**, 101 (1991);
A. Caldwell et al., Nucl. Instrum. Meth. **A 321**, 356 (1992);
A. Bernstein et al., Nucl. Instrum. Meth. **A 336**, 23 (1993).

[10] J. Andruszkow et al., Preprint DESY-92-066, DESY (1992);
ZEUS Coll., M. Derrick et al., Z. Phys. **C 63**, 391 (1994);
J. Andruszkow et al., Acta Phys. Polon. **B 32**, 2025 (2001).

[11] M. Helbich et al., Nucl. Instrum. Meth. **A 565**, 572 (2006).

[12] T. Sjöstrand et al., Comp. Phys. Comm. **135**, 238 (2001).

[13] H. Jung, *The Rapgap Monte Carlo for Deep Inelastic Scattering*. DESY, 2004, available on `http://projects.hepforge.org/rapgap/rapgap.pdf`.

[14] CTEQ Coll., H.L. Lai et al., Eur. Phys. J. **C 12**, 375 (2000).

[15] M. Glück et al., Phys. Rev. **D 46**, 1973 (1992).

[16] Particle Data Group, K. Nakamura et al., J. Phys. **G 37**, 075021 (2010 and partial update for the 2012 edition).

[17] M.G. Bowler, Z. Phys. **C 11**, 169 (1981).

[18] B. Andersson et al., Z. Phys. **C 20**, 317 (1983).

[19] B. Brun et al., GEANT3, Technical Report CERN-DD/EE/84-1, CERN, 1987.

[20] W.H. Smith, K. Tokushuku and L.W. Wiggers, *Proc. Computing in High-Energy Physics (CHEP), Annecy, France, Sept. 1992*, C. Verkerk and W. Wojcik (eds.), p. 222. CERN, Geneva, Switzerland (1992). Also in preprint DESY 92-150B.

[21] P. Allfrey et al., Nucl. Instrum. Meth. **A 580**, 1257 (2007).

[22] ZEUS Coll., S. Chekanov et al., Eur. Phys. J. **C 63**, 171 (2009).

[23] ZEUS Coll., S. Chekanov et al., Eur. Phys. J. **C 38**, 29 (2004).

[24] ZEUS Coll., S. Chekanov et al., Eur. Phys. J. **C 44**, 351 (2005).

[25] BaBar Coll., P. del Amo Sanchez et al., Phys. Rev. **D 82**, 111101 (2010).

[26] CLEO Coll., P. Avery et al., Phys. Lett. **B 331**, 236 (1994).

[27] T. Sjöstrand, Comput. Phys. Commun. **82**, 74 (1994).

[28] E. Lohrmann, Preprint hep-ex/1112.3757 (2011).

[29] J.L. Rosner, Comments Nucl. Part. Phys. **16**, 109 (1986).

[30] S. Godfrey and R. Kokoski, Phys. Rev. **D 43**, 1679 (1991).

[31] A.F. Falk and M.E. Peskin, Phys. Rev. **D 49**, 3320 (1994).

[32] OPAL Coll., K. Ackerstaff et al., Z. Phys. **C 76**, 425 (1997).

[33] Yi-Jin Pei, Z. Phys. **C 72**, 39 (1996).

[34] BaBar Coll., B. Aubert et al., Phys. Rev. Lett. **103**, 051803 (2009).

Variable	$D^0 \to K^-\pi^+$	$D^0 \to K^-\pi^+\pi^+\pi^-$
$p_T(K)$ (GeV)	> 0.45	> 0.3
$p_T(\pi)$ (GeV)	> 0.45	> 0.3
$p_T(\pi_s)$ (GeV)	> 0.1	> 0.1
$p_T(D^{*+})$ (GeV)	> 1.5	> 3
$\lvert\eta(D^{*+})\rvert$	< 1.6	< 1.6
$p_T(D^{*+})/E_\perp^{\theta>10^\circ}$	> 0.12	> 0.18
$M(D^0)$ (GeV) for $p_T(D^{*+}) < 3.25$ GeV	$1.83 - 1.90$	$1.84 - 1.89$
$M(D^0)$ (GeV) for $3.25 < p_T(D^{*+}) < 5$ GeV	$1.82 - 1.91$	$1.84 - 1.89$
$M(D^0)$ (GeV) for $5 < p_T(D^{*+}) < 8$ GeV	$1.81 - 1.92$	$1.84 - 1.89$
$M(D^0)$ (GeV) for $p_T(D^{*+}) > 8$ GeV	$1.80 - 1.93$	$1.84 - 1.89$

Table 1: *Cuts on $D^{*+} \to D^0\pi_s^+$ candidates for the decay channels $D^0 \to K^-\pi^+$ and $D^0 \to K^-\pi^+\pi^+\pi^-$.*

	HERA II	HERA I	PDG
$N(D_1^0 \to D^{*+}\pi)$	2732 ± 285	3110 ± 340	
$N(D_2^{*0} \to D^{*+}\pi)$	1798 ± 293	870 ± 170	
$N(D_2^{*0} \to D^{+}\pi)$	521 ± 88 $(S(D^+) > 3)$	690 ± 160	
$M(D_1^0)$, MeV	$2423.1 \pm 1.5^{+0.4}_{-1.0}$	$2420.5 \pm 2.1 \pm 0.9$	2421.3 ± 0.6
$\Gamma(D_1^0)$, MeV	$38.8 \pm 5.0^{+1.9}_{-5.4}$	$53.2 \pm 7.2^{+3.3}_{-4.9}$	27.1 ± 2.7
$h(D_1^0)$	$7.8^{+6.7+4.6}_{-2.7-1.8}$	$5.9^{+3.0+2.4}_{-1.7-1.0}$	
$M(D_2^{*0})$, MeV	$2462.5 \pm 2.4^{+1.3}_{-1.1}$	$2469.1 \pm 3.7^{+1.2}_{-1.3}$	2462.6 ± 0.7
$\Gamma(D_2^{*0})$, MeV	$46.6 \pm 8.1^{+5.9}_{-3.8}$	43 fixed	49.0 ± 1.4
$h(D_2^{*0})$	-1 fixed	-1 fixed	
$D_1(2430)^0/D_1^0$	1.0 fixed	1.0 fixed	
$D_0^*(2400)^0/D_2^{*0}$	1.1 ± 1.1	1.7 fixed	
Feed-downs/D_2^{*0}	0.3 ± 0.4		

Table 2: *Results of the simultaneous fit for the yields (N), masses (M), widths (Γ) and helicity parameters (h) of the D_1^0 and D_2^{*0} mesons, for the ratios of the wide states $D_1(2430)^0$ and $D_0^*(2400)^0$ to the narrow states D_1^0 and D_2^{*0}, and for the ratio of the feed-down (see text) to the $D_2^{*0} \to D^+\pi^-$. The first uncertainties are statistical and the second are systematic. The results (HERA II) are compared to earlier ZEUS results at HERA I [1] and to the PDG [16].*

	HERA II	PDG
$N(D_1^+ \to D^{*0}\pi^+)$	759 ± 183	
$N(D_2^{*+} \to D^{*0}\pi^+)$	634 ± 223	
$N(D_2^{*+} \to D^0\pi^+)$	737 ± 164	
$M(D_1^+)$, MeV	$2421.9 \pm 4.7^{+3.4}_{-1.2}$	2423.4 ± 3.1
$\Gamma(D_1^+)$, MeV	25 fixed	25 ± 6
$h(D_1^+)$	3.0 fixed	
$M(D_2^{*+})$, MeV	$2460.6 \pm 4.4^{+3.6}_{-0.8}$	2464.4 ± 1.9
$\Gamma(D_2^{*+})$, MeV	37 fixed	37 ± 6
$h(D_2^{*+})$	-1.0 fixed	

Table 3: *Results of the fit for the yields (N), masses (M), widths (Γ) and helicity parameters (h) of the D_1^+ and D_2^{*+} mesons. The first uncertainties are statistical and the second are systematic. The results are compared to those of the PDG [16].*

	total	δ_1	δ_2	δ_3	δ_4
$M(D_1^0)$, MeV	$^{+0.4}_{-1.0}$	$^{+0.4}_{-0.3}$	$^{+0.0}_{-0.8}$	$^{+0.1}_{-0.5}$	$^{+0.1}_{-0.1}$
$M(D_2^{*0})$, MeV	$^{+1.3}_{-1.1}$	$^{+0.9}_{-0.9}$	$^{+0.9}_{-0.5}$	$^{+0.2}_{-0.2}$	$^{+0.0}_{-0.1}$
$\Gamma(D_1^0)$, MeV	$^{+1.9}_{-5.4}$	$^{+1.6}_{-2.3}$	$^{+0.0}_{-1.6}$	$^{+1.0}_{-4.5}$	$^{+0.0}_{-0.0}$
$\Gamma(D_2^{*0})$, MeV	$^{+5.9}_{-3.8}$	$^{+4.0}_{-3.5}$	$^{+0.1}_{-0.2}$	$^{+4.3}_{-1.7}$	$^{+0.0}_{-0.0}$
$h(D_1^0)$	$^{+4.6}_{-1.8}$	$^{+3.1}_{-1.3}$	$^{+2.4}_{-0.3}$	$^{+2.3}_{-1.3}$	$^{+0.1}_{-0.1}$

Table 4: *Total and δ_1-δ_4 (see text) systematic uncertainties for the mass, width and helicity parameters of the neutral excited charm mesons.*

	total	δ_1	δ_2	δ_3	δ_4	δ_5
$M(D_1^+)$, MeV	$^{+3.4}_{-1.2}$	$^{+3.2}_{-0.1}$	$^{+0.0}_{-0.7}$	$^{+0.6}_{-0.1}$	$^{+0.1}_{-0.1}$	$^{+0.6}_{-0.9}$
$M(D_2^{*+})$, MeV	$^{+3.7}_{-0.8}$	$^{+1.7}_{-0.5}$	$^{+3.1}_{-0.0}$	$^{+0.4}_{-0.2}$	$^{+0.1}_{-0.1}$	$^{+0.9}_{-0.6}$

Table 5: *Total and δ_1-δ_5 (see text) systematic uncertainties for the mass, width and helicity parameters of the charged excited charm mesons.*

	total,%	δ_1, %	δ_2, %	δ_3, %	δ_4, %	δ_6, %	δ_7, %
$\mathcal{F}^{\rm extr}_{D_1^0\to D^{*+}\pi^-/D^{*+}}$	$^{+19.2}_{-14.5}$	$^{+16.4}_{-12.2}$	$^{+6.7}_{-0.0}$	$^{+3.4}_{-7.5}$	$^{+0.3}_{-0.0}$	$^{+1.5}_{-2.0}$	$^{+6.5}_{-0.0}$
$\mathcal{F}^{\rm extr}_{D_2^{*0}\to D^{*+}\pi^-/D^{*+}}$	$^{+13.5}_{-18.2}$	$^{+11.9}_{-12.9}$	$^{+3.7}_{-5.0}$	$^{+1.2}_{-11.8}$	$^{+4.9}_{-0.0}$	$^{+0.9}_{-1.5}$	$^{+0.1}_{-0.0}$
$\mathcal{F}^{\rm extr}_{D_2^{*0}\to D^{+}\pi^-/D^{+}}$	$^{+25.2}_{-17.3}$	$^{+18.6}_{-7.8}$	$^{+11.9}_{-0.0}$	$^{+5.4}_{-15.4}$	$^{+1.0}_{-0.0}$	$^{+0.5}_{-0.8}$	$^{+10.7}_{-0.0}$
$\frac{\mathcal{B}_{D_2^{*0}\to D^{+}\pi^-}}{\mathcal{B}_{D_2^{*0}\to D^{*+}\pi^-}}$	$^{+20.1}_{-19.5}$	$^{+9.9}_{-13.5}$	$^{+0.0}_{-4.7}$	$^{+9.6}_{-3.3}$	$^{+0.0}_{-0.7}$	$^{+2.3}_{-2.5}$	$^{+14.4}_{-12.7}$
$f(c\to D_1^0)$	$^{+15.8}_{-18.6}$	$^{+11.9}_{-12.9}$	$^{+3.7}_{-5.0}$	$^{+1.2}_{-11.8}$	$^{+4.9}_{-0.0}$	$^{+0.9}_{-1.5}$	$^{+8.1}_{-3.6}$
$f(c\to D_2^{*0})$	$^{+22.4}_{-15.1}$	$^{+16.1}_{-9.1}$	$^{+8.9}_{-0.0}$	$^{+4.0}_{-10.7}$	$^{+0.6}_{-0.0}$	$^{+0.6}_{-1.0}$	$^{+12.2}_{-5.3}$

Table 6: *Total and δ_1-δ_7 (see text) systematic uncertainties for extrapolated fractions, for ratios of the dominant branching fractions and for fragmentation fractions of the D_1^0 and D_2^{*0} mesons.*

	total,%	δ_1, %	δ_2, %	δ_3, %	δ_4, %	δ_5, %	δ_6, %	δ_7, %
$\mathcal{F}^{\rm extr}_{D_1^+\to D^{*0}\pi^+/D^0}$	$^{+42.6}_{-6.1}$	$^{+30.5}_{-0.0}$	$^{+18.3}_{-0.0}$	$^{+3.7}_{-2.6}$	$^{+0.0}_{-0.0}$	$^{+22.2}_{-0.0}$	$^{+1.8}_{-5.2}$	$^{+6.0}_{-1.9}$
$\mathcal{F}^{\rm extr}_{D_2^{*+}\to D^{*0}\pi^+/D^0}$	$^{+24.6}_{-14.8}$	$^{+14.7}_{-1.3}$	$^{+6.3}_{-2.4}$	$^{+1.2}_{-7.9}$	$^{+0.0}_{-0.0}$	$^{+13.5}_{-4.6}$	$^{+3.5}_{-4.0}$	$^{+12.5}_{-10.5}$
$\mathcal{F}^{\rm extr}_{D_2^{*+}\to D^{0}\pi^+/D^0}$	$^{+18.0}_{-8.0}$	$^{+13.4}_{-0.8}$	$^{+5.6}_{-4.3}$	$^{+0.2}_{-5.2}$	$^{+0.0}_{-0.0}$	$^{+3.6}_{-0.0}$	$^{+1.6}_{-1.4}$	$^{+9.8}_{-3.9}$
$\frac{\mathcal{B}_{D_2^{*+}\to D^{0}\pi^+}}{\mathcal{B}_{D_2^{*+}\to D^{*0}\pi^+}}$	$^{+23.8}_{-19.1}$	$^{+10.5}_{-8.5}$	$^{+8.3}_{-10.0}$	$^{+7.0}_{-4.7}$	$^{+0.0}_{-0.0}$	$^{+6.9}_{-9.1}$	$^{+2.7}_{-1.9}$	$^{+16.9}_{-9.3}$
$f(c\to D_1^+)$	$^{+42.7}_{-7.3}$	$^{+30.5}_{-0.0}$	$^{+18.3}_{-0.0}$	$^{+3.7}_{-2.6}$	$^{+0.0}_{-0.0}$	$^{+22.2}_{-0.0}$	$^{+1.8}_{-5.2}$	$^{+7.1}_{-4.4}$
$f(c\to D_2^{*+})$	$^{+16.7}_{-7.1}$	$^{+12.0}_{-0.0}$	$^{+1.8}_{-0.0}$	$^{+0.5}_{-5.4}$	$^{+0.0}_{-0.0}$	$^{+8.2}_{-1.2}$	$^{+2.5}_{-2.7}$	$^{+7.7}_{-3.6}$

Table 7: *Total and δ_1-δ_7 (see text) systematic uncertainties for extrapolated fractions, for ratios of the dominant branching fractions and for fragmentation fractions of the D_1^+ and D_2^{*+} mesons.*

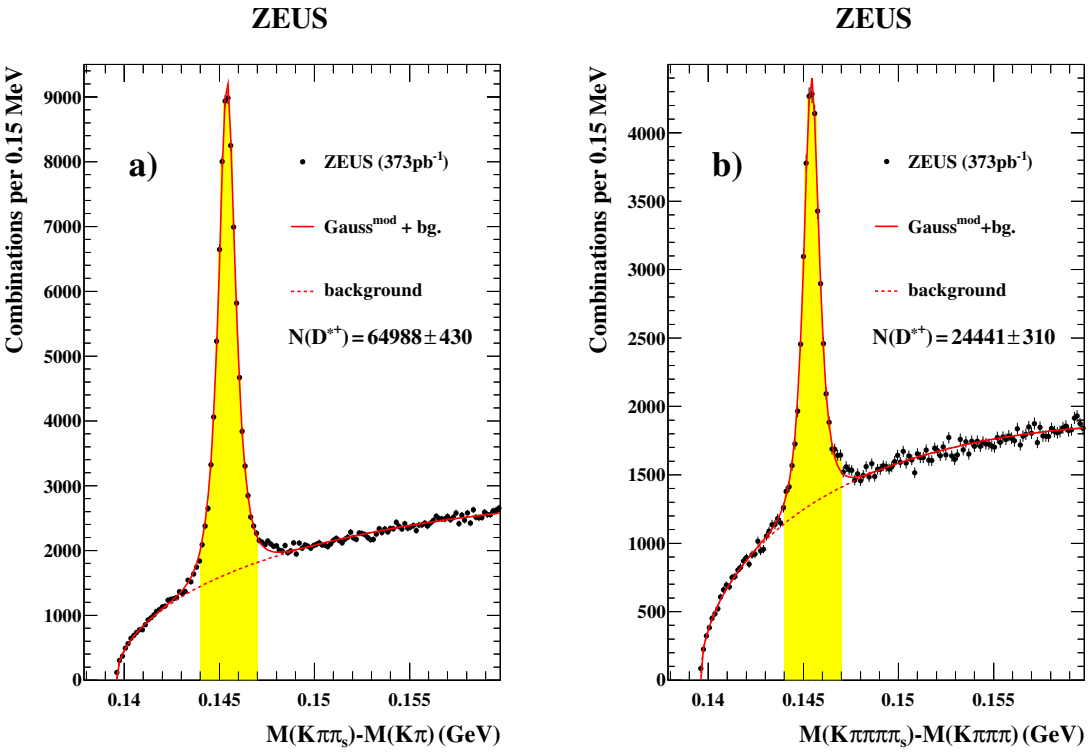

Figure 1: *The distribution of the mass difference (dots), (a) $\Delta M = M(K\pi\pi_s) - M(K\pi)$ and (b) $\Delta M = M(K\pi\pi\pi\pi_s) - M(K\pi\pi\pi)$. The solid curves are fits to the sum of a modified Gaussian function and a background function (dashed lines). Candidates from the shaded area, $0.144 - 0.147\,\mathrm{GeV}$, are used for the analysis of excited charm mesons.*

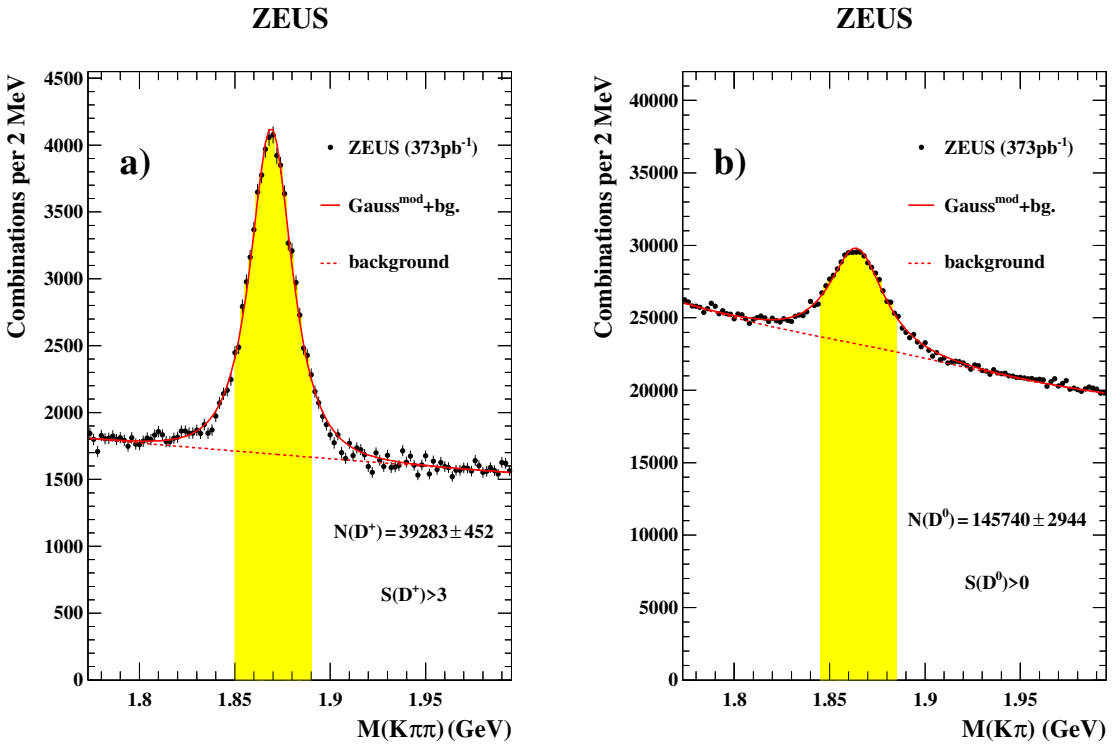

Figure 2: *The mass distributions (dots), (a) $M(K^-\pi^+\pi^+)$ for events with significance $S > 3$ and (b) $M(K^-\pi^+)$ for events with significance $S > 0$. The solid curves are fits to the sum of a modified Gaussian and a background function (dashed lines) and for (b) including also a contribution from a second broad modified Gaussian representing a reflection (see text). Candidates from the shaded areas, (a) $1.85 - 1.89\,\mathrm{GeV}$ and (b) $1.845 - 1.885\,\mathrm{GeV}$, are used for the analysis of excited charm mesons.*

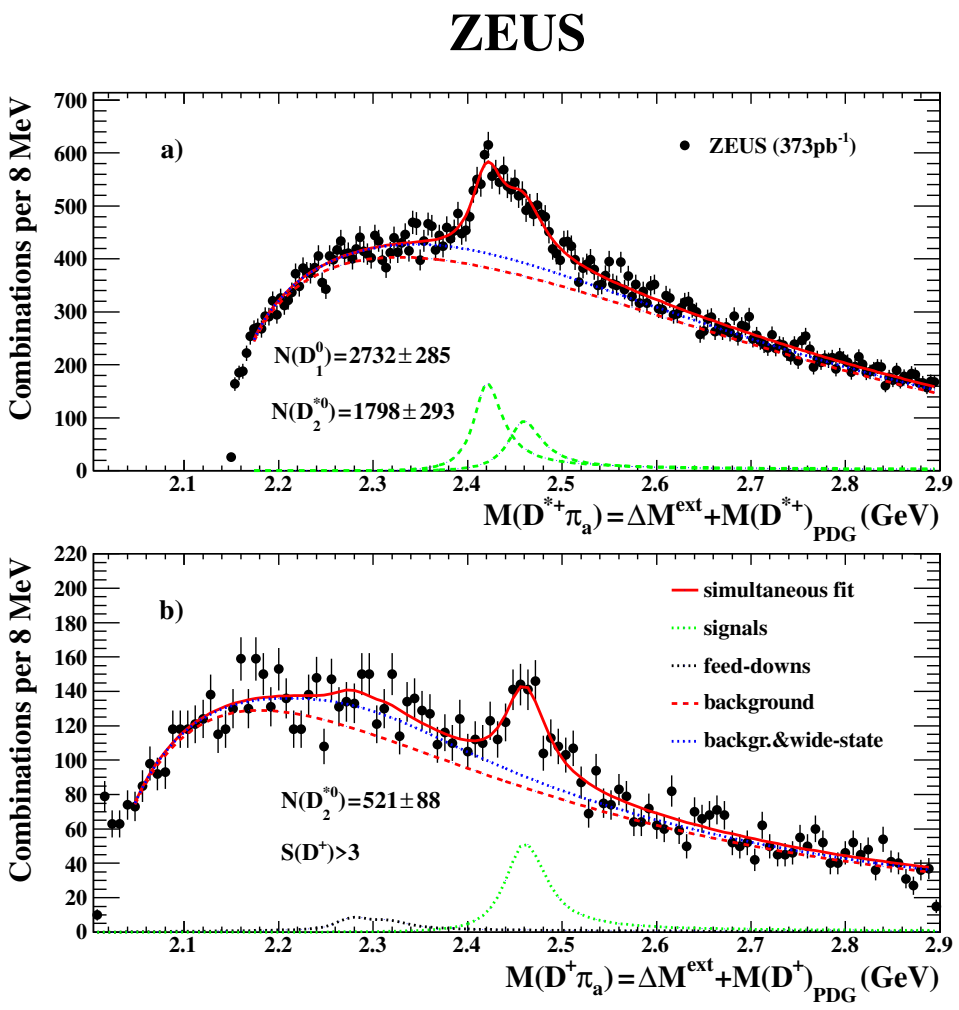

Figure 3: *The mass distributions (dots), a) $M(D^{*+}\pi_a)$ and b) $M(D^{+}\pi_a)$. The solid curves are the result of a simultaneous fit to a) D_1^0 and D_2^{*0} and to b) D_2^{*0} and feed-downs plus background function (dashed curves). The contributions of the wide states $D_1(2430)^0$ and $D_0^*(2400)^0$ are given between the dashed and dotted curves. The lowest curves are the contributions of the D_1^0, D_2^{*0} and feed-downs to the fit.*

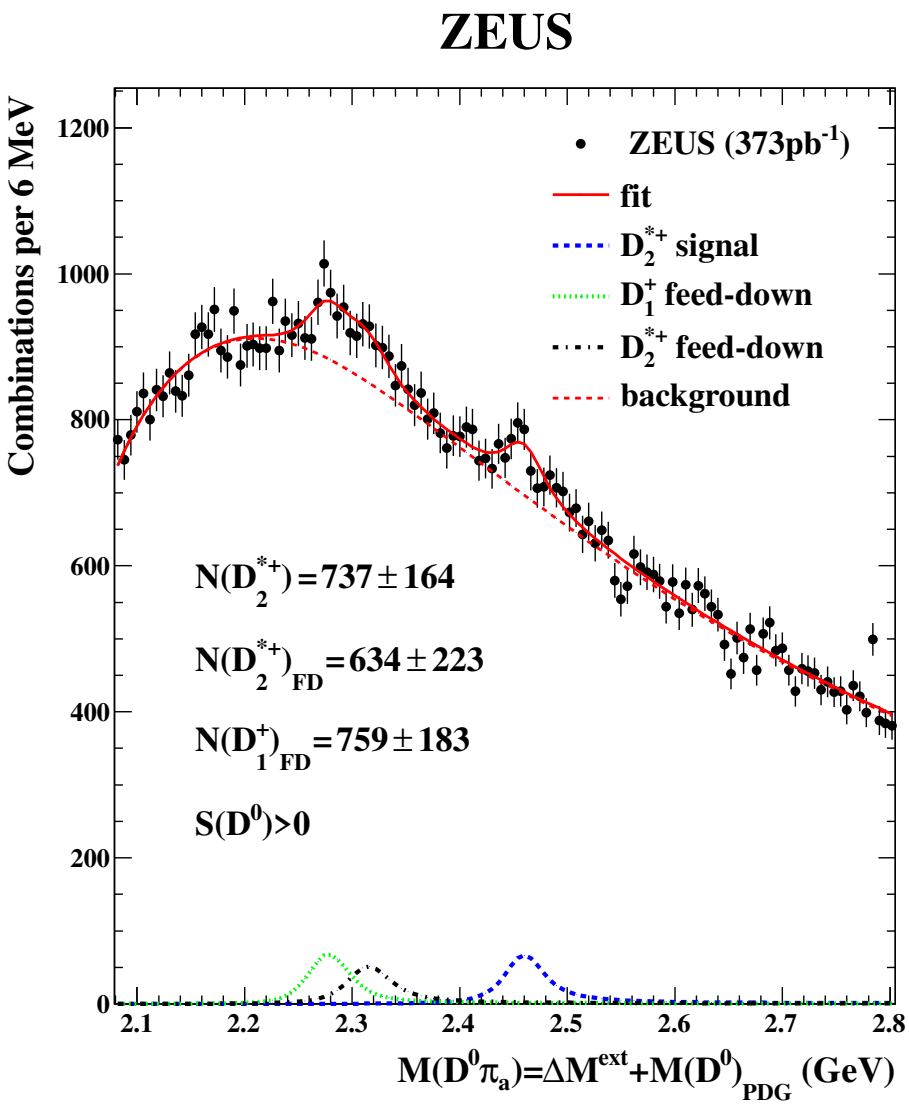

Figure 4: *The mass distribution (dots), $M(D^0\pi_a)$. The solid curve is the result of a simultaneous fit to the feed-down (FD) D_1^+ and D_2^{*+} contributions and to the D_2^{*+} signal plus background function (dashed curves). The lowest curves are the contributions of the D_1^+ and D_2^{*+} to the fit.*

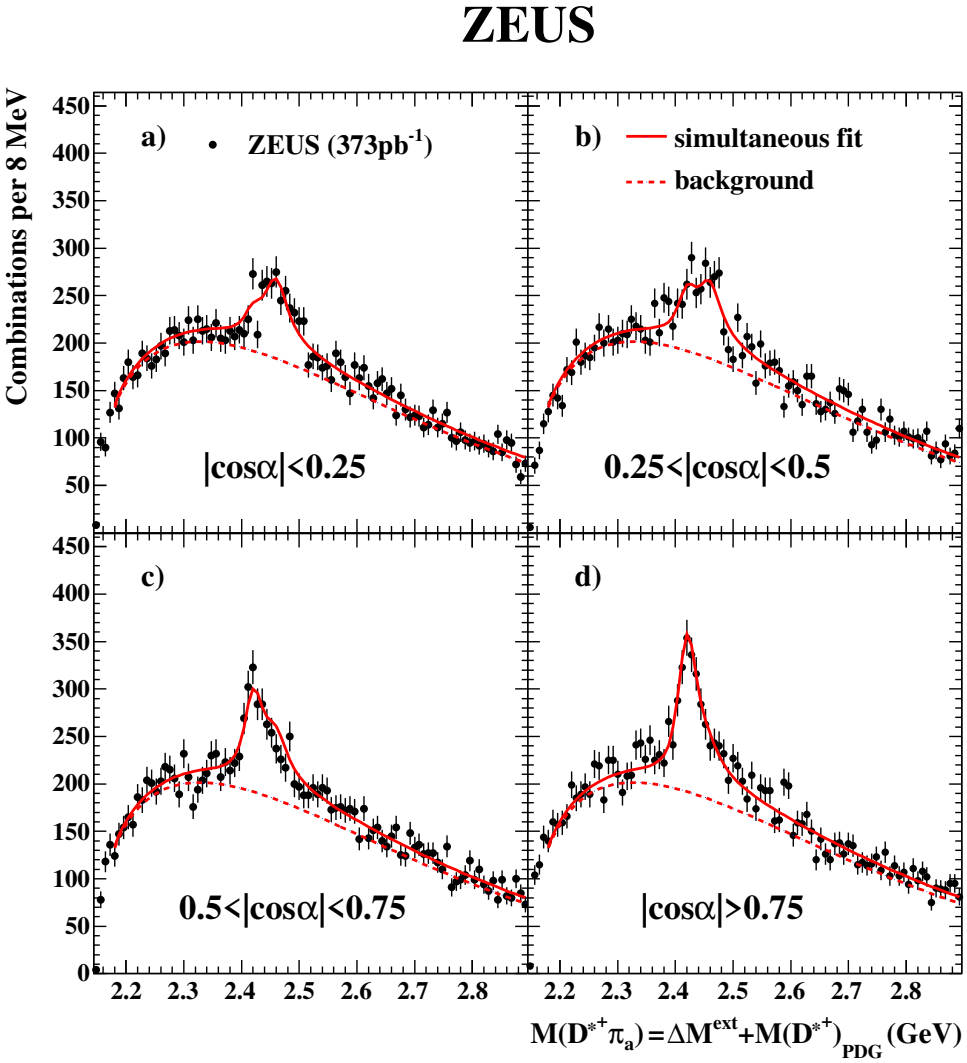

Figure 5: *The mass distributions (dots), $M(D^{*+}\pi_a)$ in four helicity intervals: (a) $|\cos\alpha| < 0.25$; (b) $0.25 < |\cos\alpha| < 0.50$; (c) $0.50 < |\cos\alpha| < 0.75$; (d) $|\cos\alpha| > 0.75$. The solid curves are the result of the simultaneous fit to D_1^0 and D_2^{*0} plus background function (dashed curves).*

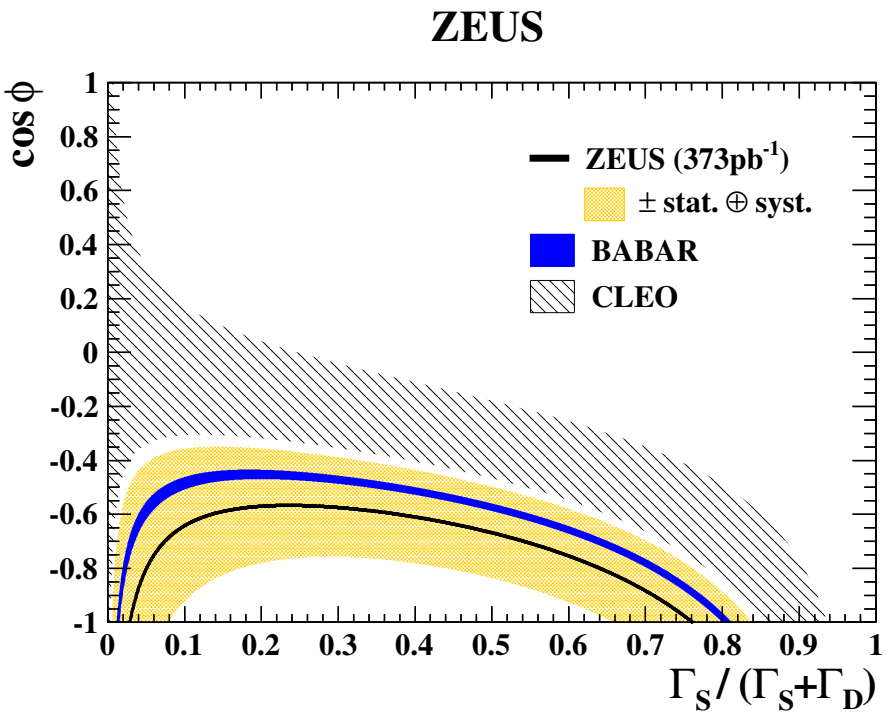

Figure 6: *The allowed region of* $\cos\phi$*, where* ϕ *is the relative phase of S- and D-wave amplitudes, versus the fraction of S-wave in the* $D_1^0 \to D^*\pi$ *decay for ZEUS, BABAR and CLEO measurements.*